Mechanisms of cell recovery: Anastasis in retinal photoreceptors

Jaya Sadda
University of Michigan

April 16, 2024

Sponsor: David N. Zacks, MD, PhD
Edna H. Perkiss Research Professor of Ophthalmology and Visual Sciences
Professor, Ophthalmology and Visual Sciences

Co-Sponsor: Cunming Duan, PhD
Professor of Molecular, Cellular, and Developmental Biology
Director, Undergraduate Program in Neuroscience

Reader: Kwoon Y. Wong, PhD
Associate Professor, Ophthalmology and Visual Sciences
Associate Professor, Molecular, Cellular & Developmental Biology

A thesis submitted in partial fulfillment of the Degree of Bachelor of Science in Neuroscience with Honors

Abstract

PURPOSE. Retinal neurodegeneration, characterized by apoptotic photoreceptor cell death, is associated with several ocular pathologies which remain the chief causes of irreversible blindness. Given the lack of reversible treatment options, neuroprotection has been an important focus of investigation. Recent studies have shown that apoptosis can be halted and reversed in a process known as "*anastasis"*. This study aims to determine if anastasis can occur in photoreceptors and if so, what may control this mechanistically.

METHODS. 661W mouse photoreceptor cells were treated with staurosporine (STS) for 15 hours to induce apoptosis. The drug was subsequently removed and replaced with fresh media, and cells were allowed to recover for 24 or 48 hours. MTT and Crystal violet assays were performed to assess cell viability and proliferation/morphology, respectively. PARP/cleaved-PARP expression in cells was measured using Western blotting. RT-PCR was conducted to evaluate relative mRNA expression of three early-response genes associated with anastasis (IER5, EGR1, FOS).

RESULTS. After 48 hours of recovery in fresh media, photoreceptors that exhibited hallmarks of apoptosis, regained healthy cell morphology. PARP-1 (mean Fold change=0.968, $p<0.05$) and Cleaved-PARP-1 (mean Fold change=0.685, $p<0.05$) protein expression significantly decreased in recovery cells, matching that of untreated controls. Compared to treatment-induced apoptotic cells, recovered cells demonstrated increased cell proliferation and enrichment of IER5, EGR1, and FOS, early-response genes associated with anastasis (Mean relative mRNA expression: IER5: 5.860, $p<0.05$; EGR1: 0.899, $p<0.05$; FOS: 3.000, $p<0.05$).

CONCLUSIONS. Our data suggests that photoreceptors can recover from apoptosis, and that they show the hallmark signs of anastasis.

Table of Contents

Abstract ..... *i*

Table of Contents ..... *ii*

Scientific Acknowledgements ..... *iii*

Personal Acknowledgements ..... *v*

Introduction *1*
- ~ Introduction.
- ~ Overview of Cell Death – with a focus on Apoptosis.
- ~ Relevance.
- ~ Anastasis in Cancer Cells: Literature Review.
- ~ Previous Photoreceptor Studies: Rescue & Neuroprotection — Why Anastasis.
- ~ Present Study.

Methods *17*
- ~ 661W Mouse Retinal Photoreceptors & Cell Culture.
- ~ Drug Treatment.
- ~ MTT Assay.
- ~ Crystal Violet: Assay & Imaging.
- ~ RNA Isolation, cDNA Preparation, & qRT-PCR.
- ~ Western Blot.
- ~ Statistical Analysis Methods.

Results *22*
- ~ MTT: Cell Viability Assay for Concentration Kinetics.
- ~ Crystal Violet Staining: Cell Proliferation Assay for Concentration Kinetics.
- ~ Morphology.
- ~ Crystal Violet Assay of Cells following 24 hours of Recovery.
- ~ Crystal Violet Assay of Cells following 48 hours of Recovery.
- ~ Western Blot & Changes in PARP Expression after 48 hours of Recovery.
- ~ Real-Time Polymerase Chain Reaction (RT-PCR) of IER5, EGR1, & FOS after 48 hours of Recovery.

Discussion *33*

References *38*

Appendix *48*

Scientific Acknowledgements

The data presented in this thesis resulted from a close collaboration with Bhavneet Kaur, PhD, a postdoctoral fellow and researcher in the Zacks Lab at the University of Michigan, Kellogg Eye Center. Dr. Kaur has granted me permission to also incorporate some of the data she collected in this summary. For all completed experiments, we performed similar experiments and we aggregated the results to increase the power of our analysis. When obtaining results for all the experiments, I performed 3 technical replicates — as did Dr. Kaur. Our data were also aggregated to include biological replicates (in which experiments where performed at different times by different people). All figures (excluding Crystal Violet imaging and Western Blot imaging) include our combined data.

FIGURE #	PERSON RESPONSIBLE FOR ILLUSTRATED EXPERIMENT
1	Figure from Stillwell, 2016.
2	Figure modified from Ketelut-Carneiro & Fitzgerald, 2022.
3	Figure from Tang et al., 2018.
4	Bhavneet Kaur selected and compiled a list of a few anastasis markers to further investigate based on Sun et al., 2017. I created the figure.
5	I created and adapted the figure based on hallmarks of anastasis identified by Tang et al., 2018.
6	I created the figure.
7,8	Bhavneet Kaur and I each separately carried out the experiments presented in these figures. Our data was compiled and presented together in the figures. I carried out the statistical analysis and created the figures in GraphPad Prism.
9,10	I performed the experiment. Bhavneet Kaur and I took the images together.
11,12	Bhavneet Kaur and I each separately carried out the experiments presented in these figures. Our data was compiled and presented together in the figures. I carried out the statistical analysis and created the figures in GraphPad Prism.
13	I performed the experiment. Bhavneet Kaur took the image, and I labelled it for the figure.
14	Bhavneet Kaur and I each separately carried out the experiments presented in this figure. Our data was compiled and presented together in the figure. I carried out the statistical analysis and created the figure in GraphPad Prism.
15	Bhavneet Kaur and I each separately carried out the experiments presented in this figure. Our data was compiled and presented together in the figure. I carried out the statistical analysis and created the figure in GraphPad Prism.

--

I would also like to thank Bhavneet Kaur, PhD, Bruna Miglioranza Scavuzzi, PhD, and the entire Zacks lab for allowing me to utilize their experimental protocols and laboratory resources. I am deeply grateful to David Zacks, MD, PhD, and Bhavneet for their guidance throughout this entire project.

--

Personal Acknowledgements

I would like to start by thanking my advisor and principal investigator (PI), **David Zacks**, MD, PhD for not only welcoming me into your lab, but also for meeting with me biweekly to discuss my research and for all your time reading drafts to make this thesis the best it could be. I am grateful for your continuous mentorship and support over the past three years.

Bhavneet, thank you for mentoring me, teaching me experiment techniques, and for accommodating me into your lab schedule with flexibility and patience, and answering all my questions along the way.

To **Amma** & **Nanna**, thank you for always believing in me, loving me unconditionally, and providing endless support throughout my journey. I am forever grateful for the time, resources, and patience you have invested in me – and most of all for always encouraging me to pursue my dreams (and for all the phone calls).

To **Neel**, my best friend for life, what would I do without your motivational pep talks over Facetime and our daily updates text chains. Thank you for always keeping me grounded, getting my head in the game, and being a source of comic relief.

To **Chinnu** & **Teja**: **Chinnu**… I think I owe you a hundred thousand Facetime minutes over the past four years. Thank you for always being an open ear. **Teja**, I think Chinnu and I Facetime enough for the three of us. But your occasional text message always makes my day.

To **Emma** & **Lucy**, my rocks this year. Thank you for sticking with me through all the stress and crazy, for searching the entire UGLI to find me to bring me hairbrushes & Trader Joe's snacks, and for your never-ending encouragement. **Emma**, what would I have done without all the check-in texts, power poses, and pictures updates of Otis. **Lucy**, you never fail to keep me laughing through it all & your perfect responses when I am stressed beyond belief get me through it.

Lastly, thank you to all my friends & family who have supported me during my time at the University of Michigan, and to **802** (Cass, Emma, & Lucy) for being the best place to come back to after hibernating in the library.

Introduction

Introduction.

The typical mammalian retina contains a variety of neuron types, all which play a role in the transmission of visual information to the brain. The retina converts a light stimulus into a nerve impulse, which is carried to the brain via the optic nerve, making it a key functional component of the central nervous system (Marchesi et al., 2021). Of particular relevance to this study are retinal photoreceptors (PR) cells because of their involvement in the pathology of neurodegenerative disorders. Photoreceptors, specifically rods and cones, are specialized light-sensitive neurons that serve as the initial components of the visual system. They are found at the back of the retina, adjacent to the retinal pigment epithelium (RPE) and convert light stimuli into electrical signals to further activate the visual pathway (Liton et al., 2023).

Retinal neurodegeneration is related to several ocular pathologies (including glaucoma, age-related macular degeneration (AMD), and diabetic retinopathy (DR)), which remain the chief and most frequent causes of irreversible blindness. Such diseases result in the progressive degeneration and death of retinal cells, ultimately leading to vision loss (Schmidt et al., 2008). Whilst the causes and exact clinical classifications of each retinal disease differ, previous research proposes that they all do share some of the molecular pathways which ultimately result in cell death (Murakami et al., 2013). Cell death in the retina can be induced by several factors such as oxidative stress, DNA damage from ultraviolet light A (UVA), retinal phototoxicity, and metabolic stress (Yu et al., 2022; Olivares-González et al., 2021; Françon & Torriglia, 2023). Such factors trigger death pathways, including apoptosis (Type I), autophagy (Type II), and necrosis (necroptosis) (Type III) (Murakami et al., 2013). The former is of particular interest in the present study, with particular emphasis on the photoreceptor cell.

Overview of Cell Death – with a focus on Apoptosis.

As aforementioned, three main pathways (apoptosis, autophagy, and necrosis) are associated with cell death. Apoptosis has typically been considered the primary pathway by which photoreceptors die in response to stress and other noxious stimuli (Chinskey et al., 2014). However, current studies continue to examine the roles of other processes – namely, necrosis, autophagy, and inflammation – in contributing to cell death (Chinskey et al., 2014). This study

focuses on the apoptotic pathway, as it has been studied extensively and is the primary pathway implicated in cell death from stress.

Apoptosis, often deemed “programmed” or “signal dependent” cell death, is a critical component of a multitude of biological processes (Green and Llambi, 2015). Dysregulation of apoptosis may result in excessive or insufficient activation of the apoptotic pathway, playing a key role in various conditions including several types of cancer, neurodegenerative diseases, and ischemic damage (Elmore, 2007).

A hallmark and key physical identifying feature of apoptosis is its distinct morphology which has been thoroughly examined via light and electron microscopy (Elmore, 2007). As opposed to other types of cell death, apoptosis is characterized by pyknosis, the degeneration of a nucleus due to chromatin condensation (Harvey, 2012). This leads to cell shrinkage, and these smaller cells have a denser cytoplasm and more tightly packed organelles. Additionally, membrane blebbing is observed in late-phase apoptotic cells (Coleman et al., 2001; Green and Llambi, 2015). Morphologically, blebbing causes asymmetrical protrusions and bulges of the plasma membrane and these membrane blebs, along with some cytoplasm and nuclear fragments, eventually break away from the cell forming apoptotic bodies (Stillwell, 2016). These distinct physical changes which occur during apoptosis are orchestrated by caspase activation, which subsequently promotes ROCK1 protein to form blebs and transfer DNA fragments into blebs (Coleman et al., 2001). On the subcellular level, apoptosis causes karyorrhexis or nuclear fragmentation which results in the breakup of chromatin. Such changes can be identified via electron microscopy (Harvey, 2012).

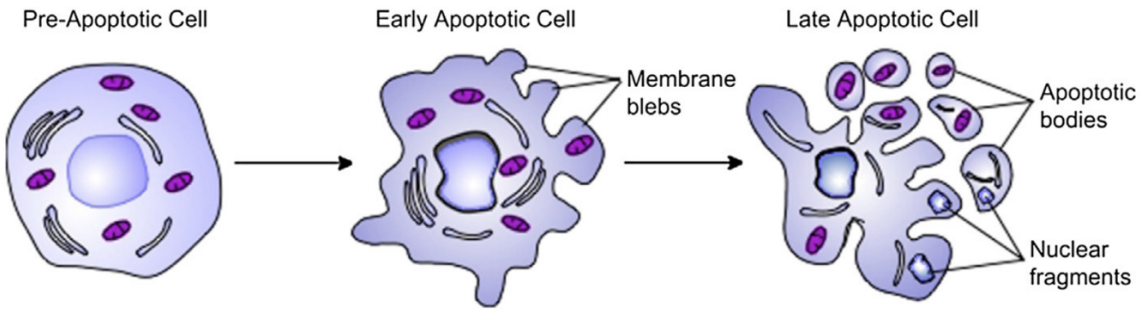

Figure 1. Morphological Changes (Membrane Blebbing) during Apoptosis (Stillwell, 2016).

Moreover, many previous studies frequently divide apoptosis into the intrinsic and extrinsic pathways. The intrinsic (mitochondrial) pathway is the most common of the two

mechanisms in vertebrates (Green and Llambi, 2015). Cellular stressors – such as DNA damage, growth factor deprivation, endoplasmic reticulum (ER) stress, excessive reactive oxygen species (ROS), and oncogene activation – activate it (Green and Llambi, 2015; Ketelut-Carneiro and Fitzgerald, 2022). In this pathway, multiple BCL-2 family proapoptotic protein interactions tightly modulate apoptosis by regulating mitochondrial outer membrane permeabilization (MOMP) (Ketelut-Carneiro and Fitzgerald, 2022). Typically, cytochrome *c* is strictly located in the mitochondrial intermembrane space but, MOMP inadvertently triggers cytochrome *c* release to the cytoplasm from the mitochondrial intermembrane space (Chipuk et al., 2006; Green and Llambi, 2015). Here cytochrome *c* binds to apoptotic protease-activating factor (APAF-1) prompting the conversion of dATP to dADP of the Apaf1 cofactor, enabling 7 APAF1–dATP–cytochrome-*c* units to oligomerize into an active apoptosome (Green and Llambi, 2015). Furthermore, the APAF-1 apoptosome comprises of caspase recruitment domains (CARD) which bind to pro-caspase-9 CARD, activating it. Activated caspase-9 then cleaves procaspase-3 and pro-caspase-7, leading to the execution phase and finally cell death (Ketelut-Carneiro and Fitzgerald, 2022).

The extrinsic (death receptor-mediated) pathway is categorized by death receptors on the plasma membrane which respond to extracellular signals from neighboring cells, the environment, or the immune system, and induce death (Ketelut-Carneiro and Fitzgerald, 2022). Specific cell surface receptors recognize their corresponding death ligand, which include Fas ligand (FASL), tumor necrosis factor (TNF), and TNF-related apoptosis-inducing ligand (TRAIL-1/2). Upon ligation, the intracellular region of such death receptors mobilizes adaptor molecules and other cytoplasmic factors, which interact and use the death-inducing signaling complex (DISC) to activate pro-caspase-8 (Green and Llambi, 2015; Ketelut-Carneiro and Fitzgerald, 2022). Activated caspase-8 then activates caspase-3 and caspase-7 by cleaving their inactivated pro- forms, allowing them to initiate the execution pathway and elicit cell death (Ketelut-Carneiro and Fitzgerald, 2022).

The intrinsic and extrinsic pathways both end at caspase-3 activation, thus converging on the final pathway of apoptosis: the execution phase. Caspases- 3, 6, and 7 operate as "executioner" (effector) caspases, activating cytoplasmic endonuclease and proteases which degrade nuclear material, and cytoskeletal and nuclear proteins respectively (Slee et al., 2001; Elmore, 2007; Holland and Cleveland, 2012). This final pathway is what triggers the distinctive

biochemical and morphological changes of apoptosis including blebbing and cell shrinkage, along with phagocytosis of apoptotic bodies (ApoBDs) by macrophages and parenchymal cells (Elmore, 2007). Caspase activation is defined by quick and massive cellular demolition through multiple caspase-mediated apoptotic pathways because it amplifies death signals (Riedl and Shi, 2004). Ultimately, caspase cascades cause organelle fragmentation, DNA damage caused by DNases, and further increased MOMP due to BID cleavage (Taylor et al., 2008; Green and Kroemer, 2004; Chipuk et al., 2006). The robust damage triggered by caspases is why the execution (caspase-mediated) phase was formerly deemed irreversible (Riedl and Shi, 2004; Taylor et al., 2008; Tang et al., 2018).

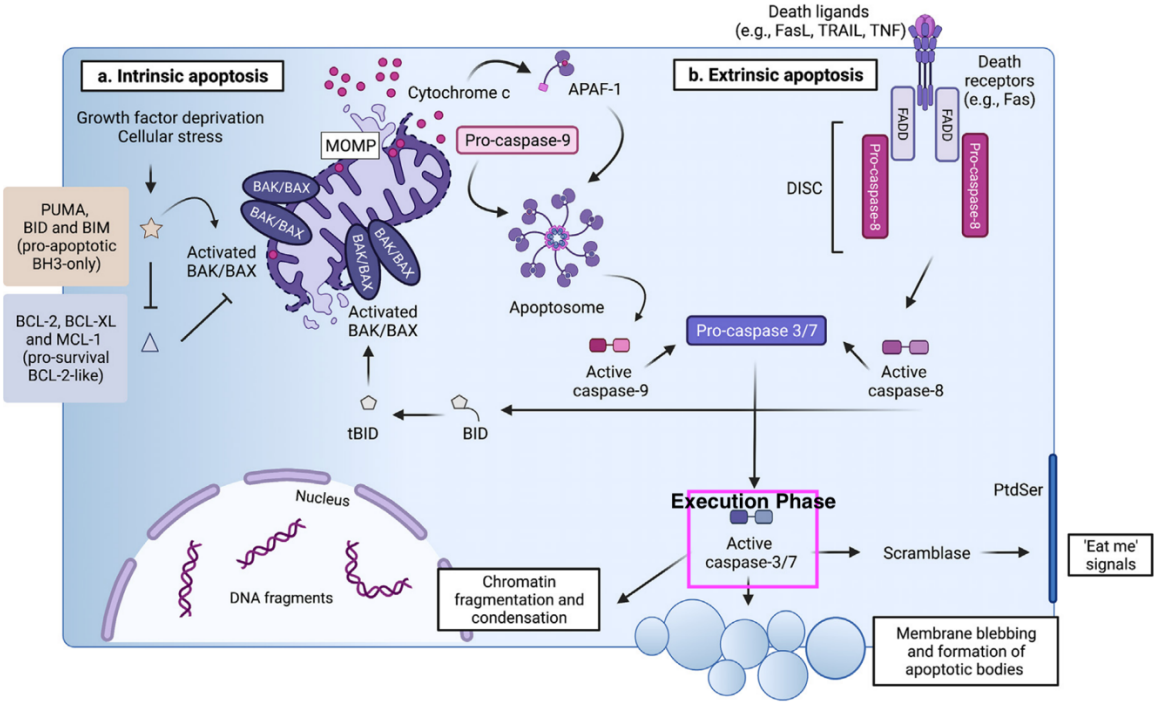

Figure 2. Molecular Mechanisms of the Intrinsic and Extrinsic Pathways of Apoptosis. Pathways converge at activation of caspase-3 and caspase-7, the onset of the execution phase (Modified from Ketelut-Carneiro and Fitzgerald, 2022).

Key points along the apoptotic pathway have been extensively studied and later classified as apoptotic markers. Cleaved Caspase-3 and cleaved Poly(ADP-ribose) polymerase (PARP), once activated, are essential proteins which play crucial roles along the apoptotic pathway. Hence, they are considered as biomarkers of apoptosis and can be assessed to reveal whether apoptosis is occurring and to what extent (Karamitopoulou et al., 2007; Chaitanya et al., 2010; Ward et al., 2008). Activated Caspase-3 is part of the execution phase and is responsible for the

cleavage of many downstream targets, resulting in the previously mentioned prototypical apoptosis morphology. Caspase-3 facilitated cleavage of the inhibitor of caspase-activated DNAse (ICAD) pathway ultimately prompts chromatin condensation and DNA fragmentation (Eskandari and Eaves, 2022; Enari et al., 1998; Larsen and Sørensen, 2017). In addition, ROCK1 cleavage by caspase-3 yields cell shrinkage (Eskandari and Eaves, 2022; Elmore, 2007). Caspase-3, along with caspase-7, is also a player in yet another typical event: the proteolytic cleavage of poly(ADP-ribose) polymerase-1 (PARP-1) (Los et al., 2002). PARP-1 is a nuclear enzyme which, under normal conditions, contributes to DNA stability and transcriptional regulation via the DNA base excision repair (BER) system (Los et al., 2002; Hong, 2024). Cellular stresses prompt PARP-1 to attach poly(ADP ribose) polymers to repair DNA damage (Chaitanya et al., 2010). However, caspase mediated cleavage of PARP-1, within the nuclear localization signal adjacent to the DNA-binding domain, terminates its activity and subsequently attenuates DNA repair (Mashimo et al., 2021). PARP-1 is cleaved into 2 fragments: a 24-kDa fragment and an 89-kDa fragment (Mashimo et al., 2021). The latter bears the catalytic domain and is released to the cytosol due to diminished DNA binding affinity (Chaitanya et al., 2010). On the other hand: the 24-kDa fragment remains in the nucleus and irreversibly binds to damaged DNA regions, preventing different PARP and other DNA repair enzymes from binding, and further suppressing chromosome repair (Chaitanya et al., 2010).

Relevance.

The above discussion regarding cell death expressed that poorly regulated apoptosis is an essential determinant in a variety of neurodegenerative diseases and some cancers, among other pathologies (Elmore, 2007). Put simply, cancer is a disease characterized by failed apoptosis. Unable to respond appropriately to cellular growth control signals, cells divide uncontrollably (Cooper, 2000). This continuous, unregulated proliferation of cancer cells leads to abnormalities in both cell behavior and accumulation resulting in tumors and tissue masses (Cooper, 2000). Prior studies indicate the survivability and viability of various cell types, even after the appearance of morphological and biochemical hallmarks of cell death (Mohammed et al., 2022; Acuner Ozbabacan et al., 2012). One study, perhaps the ‘pioneering’ study of anastasis, by Tang et. al found that ethanol treated HeLa cervical cancer cells could survive apoptosis induction (Mohammed et al., 2022; Tang et al., 2018). Interestingly, it was not that removal of ethanol

prevented the induction of apoptosis from occurring at all; indeed, characteristic features of apoptosis (MOMP, activated caspase-3, and DNA damage) were present (Mohammed et al., 2022; Tang et al., 2018). Apoptosis was triggered, but the pathway did not go to completion. The HeLa cancer cells reverted to their typical morphology and cancer cell function was also restored (Mohammed et al., 2022; Tang et al., 2018). Thus, Tang et. al coined the term "*anastasis*" (resurrection), to describe the phenomenon of survival and rescue of cells on the verge of death (Tang et al., 2018).

Seeing as anastasis is a prospective mechanism for cell recovery, it also emerges as an area of interest in retinal neuroprotection. As previously mentioned, retinal neurodegenerative disease prognoses are all based on the loss of photoreceptor cells (Schmidt et al., 2008). Research in ophthalmological interventions for such conditions such as glaucoma, AMD, and DR have advanced, and there are some measures which attempt at slowing disease progression. But, to date, there are no actually curative treatments for true disease prevention nor for disease reversal (Murakami et al., 2013; Fabre et al., 2022; Patel et al., 2023). Consequently, retinal neuroprotection remains a critical area of research, and anastasis could be a new avenue for potential treatment mechanism of which to investigate. Stimulating anastasis may allow for photoreceptor preservation and survival, assisting in prolonged retinal function (Tang et al., 2018). Much of the research on anastasis has been done in cancer cells, and therefore it has not been thoroughly studied in photoreceptors. To begin investigation of potential anastasis in PR cells, this study first enlists in a critical review of anastasis literature.

Anastasis in Cancer Cells: Literature Review.

REVERSIBILITY OF APOPTOSIS

Until recent times, apoptosis has been considered an extremely rapid and largely irreversible process, deemed to "commit a cell to death" within 10 to 15 minutes of pathway initiation (Elmore, 2007; Green, 2005). Executioner caspase activation, in particular, was considered the "point of no return," in which cells that reached this stage supposedly had no chance of survival (Sun et al., 2017; Green and Kroemer, 1998). However, research into cancer cell survival during chemotherapy has challenged the accuracy of previous theories. Typically, reemergence of cancer during and after treatment has been linked to: inadequate drug penetration into tumors, apoptotic pathway deficiency, or anticancer drug resistance (Minchinton and

Tannock, 2006; Letai, 2008; Dean et al., 2005), but newer research highlights a different possibility: the reversibility of apoptosis after toxin removal, even after apoptotic pathway initiation occurs.

In one study, Tang et al. triggered apoptosis in HeLa cells following treatment with jasplakinolide, evidenced by: morphological changes in cells' cytoplasm and nucleus, protease caspase activation, and cleavage of pro-caspase-3 (Tang et al., 2009). Upon wash and removal of the drug, the cells were re-cultured in fresh media for 24 hours, and it was found that HeLa cells could survive even after induction of apoptosis: **92%** of the 96% of cells which exhibited shrinkage and were considered apoptotic, recovered their normal morphology within a recovery period of 24 hours (Tang et al., 2009). Moreover within 72 hours and 168 hours of recovery, treated HeLa cells showed no significant difference in caspase and mitochondria activity, respectively, compared to untreated controls. Cells were also able to proliferate following toxin removal, even though caspase-3 (an execution caspase) had been activated (Tang et al., 2009). Normal levels of caspase and mitochondrial activity, along with evidence of cell division suggest that HeLa cells which were apoptotic, recovered their cancer cell function; the characteristic morphological and biochemical hallmarks of apoptosis which were present during treatment disappeared (Tang et al., 2009). Similar results have been observed across different cancer cell lines and using different drugs, indicating reversibility of apoptosis is a common occurrence amongst cancer cells.

SIGNIFICANCE OF ANASTASIS

Anastasis (Αναστάσης), Greek for "rising to life" or "resurrection," is defined as "a natural cell recovery phenomenon that rescues cells from the brink of death" (Tang et al., 2018). Initial findings from Tang et al. spurred research in the novel field of anastasis because, contrary to prior belief, they showed that cancer cells could regain their function even after the onset of the apoptotic pathway (Tang et al., 2009; Sun and Montell, 2017). Further investigation suggests that anastasis may apply to other types of cell death and is a principle of intrinsic recovery: ceasing death stimulation is adequate to recover cell function *in vitro* and *in vivo* (Tang et al., 2018).

Interestingly, research also found that the percentage of cells exhibiting nuclear fragmentation significantly increased the longer they were treated with the apoptotic reagent

(Tang et al., 2009). The degree of nuclear fragmentation inversely corresponds to the recuperation and capacity of cell proliferation following the recovery period, indicating that the former may be the "apoptotic landmark event," whereafter apoptosis truly becomes irreversible (Tang et al., 2009). This finding raises a potential question which requires further investigation if anastasis is to be the basis of neurodegenerative therapies: how late, is too late, for cell function recovery? What is the final checkpoint between anastasis and cell death?

MECHANISM OF ANASTASIS

The exact mechanism of anastasis is still uncertain, but studies have proposed various strategies which cells could employ to regain normal morphology and function ― based on the apoptotic features present in cells at a given point in time and whether recovery still occurs once that part of the pathway is reached (Figure 3). Single cell live microscopy studies established that cells showing signs of cytochrome *c* release into the cytoplasm, mitochondrial fragmentation, and membrane blebbing (occurring downstream of caspase activation of ROCK1), were able to recover (Tang et al., 2018; Tang et al., 2015). Similar reversibility of apoptosis following cytochrome *c* release and caspase-3 activation is also observed *in vivo* in apoptotic cardiomyocytes (Tang et al., 2018; Narula et al., 1999). Despite this caspase-3 activation, cardiomyocytes exhibited normal nuclear morphology indicating apoptosis did not go to completion (Kanoh et al., 1999).

Whilst evidence alludes to the viability of anastasis even after cytochrome *c* release and mitochondrial damage, how this is possible requires clarification considering the mitochondria provides the cell with necessary energy required for cellular functions. Thus, anastatic cells must have at least some mitochondrial function remaining to provide energy at the start of the recovery process. Tang et al. propose that energy requirements are fulfilled by surviving, semi-functional mitochondria, raising the notion that cytochrome *c* release is not an "all-or-nothing" circumstance as previously thought (Tang et al., 2018; Goldstein et al., 2000). Now, incomplete mitochondrial outer membrane permeabilization (iMOMP) demonstrates only partial cytochrome *c* release causing only minimal caspase activation, which is inadequate to fully execute cell death (Ichim et al., 2015). The exact mechanisms which permit outer membrane integrity are still unclear, but upregulation of antiapoptotic BCL-2 family proteins potentiates mitochondrial viability and survival (Mohammed et al., 2022; Frenzel et al., 2009). Mitochondria in anastatic

cells eventually do indicate recovery by the late stage; fragments re-fuse together, allowing normal tubular structure to reform and they can once again carry out metabolic processes, allowing for further cell recovery (Tang et al., 2018; Tang et al., 2009; Tang et al., 2017; Tang et al., 2012).

Even more recently, it is suspected that anastatic cells upregulate expression of certain candidate genes to 'clean up' and reverse the initial MOMP-caused damage. Degradation of damaged mitochondria and removal of residual cytosolic cytochrome *c* occurs via autophagy (Ding and Yin, 2012; Mohammed et al., 2022). The autophagic proteins, ATG12 and SQSTM1, which mediate mitophagy and mitochondrial homeostasis were found to be upregulated when no caspase pathway activity was present (Tang et al., 2018; Radoshevich et al., 2010; Villa et al., 2017; Geisler et al., 2010; Okatsu et al., 2010). This indicates that nonfunctional mitochondria are eliminated by anastatic cells via mitophagy as part of the recovery mechanism. ATG12 also drives cytochrome *c* degradation and heat shock protein (HSP) chaperones (HSP27 and HSP70) inhibit any further release from the mitochondria (Mohammed et al., 2022; Colell et al., 2007; Gama et al., 2014; Paul et al., 2002; Mosser et al., 2000). Furthermore, studies establish that various heat shock proteins and heme oxygenase prevent DNA destruction, additional leakage of apoptogenic agents, and eliminate free radicals, to reinstate healthy activity (Tang et al., 2018; Ravagnan et al., 2001; Gurbuxani et al., 2003; Kalinowska et al., 2005; Gozzelino et al., 2010).

As previously stated, newer evidence points to the reversibility of apoptosis even after caspase activation during the execution phase. Tang HL, et al. determined, using time-lapse live cell microscopy and a caspase biosensor, that human cervical cancer cells which showed caspase activation after ethanol-based apoptosis induction, were able to recover (Tang et al., 2018; Tang et al., 2012). The cells reversed mitochondrial fragmentation, membrane blebbing, and pyknosis to regain normal structure and function (Tang et al., 2018; Tang et al., 2015; Tang et al., 2012). It is proposed that recovery is achieved through HSP mediated suppression of caspase-3, caspase-7, and caspase-9 activity. HSP27 binds inactivated procaspase-3, thus preventing caspase-9 from cleaving it to caspase-3, the active form (Tang et al., 2018; Pandey et al., 2000). HSP27, HSP70, and HSP90 halt apoptosome formation, ensuing inactivation of caspase-9 and the rest of the caspase cascade (Figures 2-3), (Tang et al., 2018; Pandey et al., 2000; Beere et al., 2000).

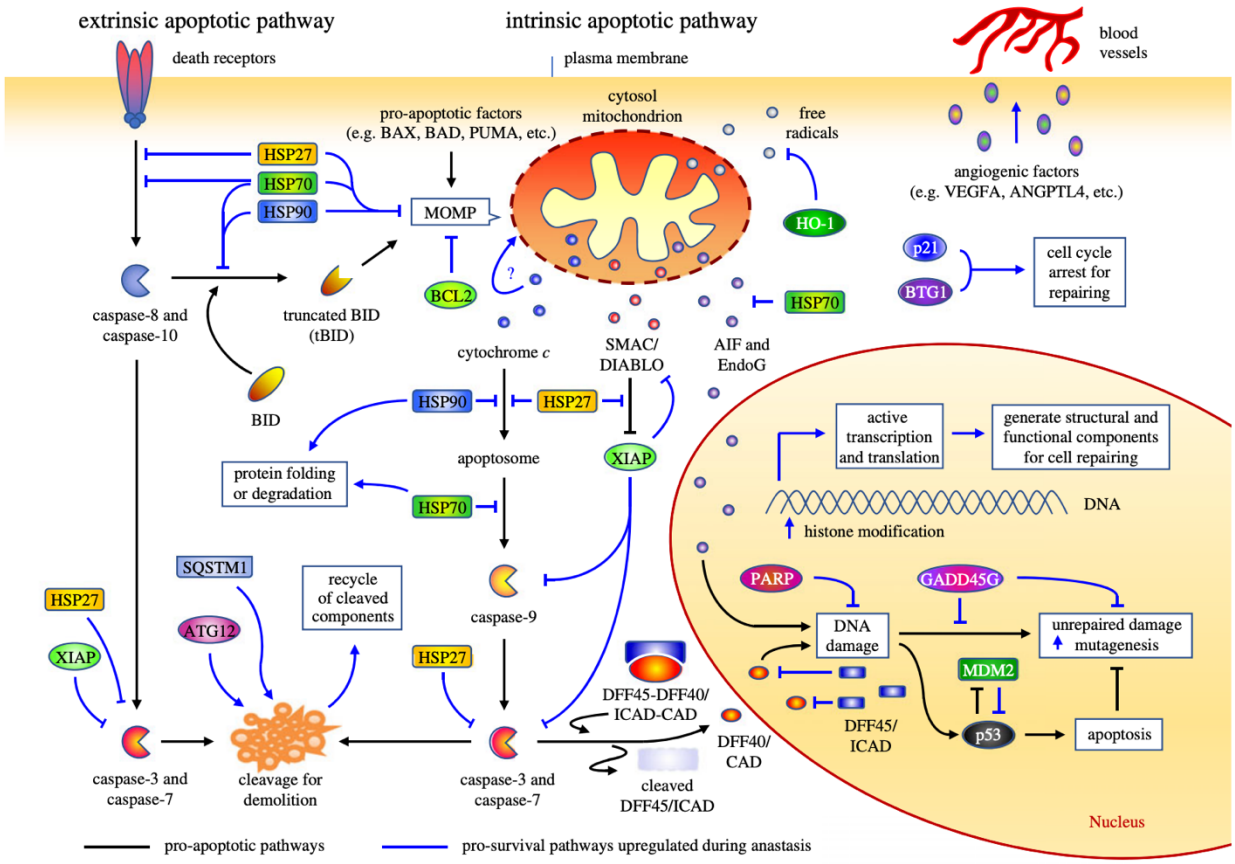

Figure 3. Proposed mechanism of anastasis leading to cell recovery by Tang et al. Anastatic cells act to terminate and subsequently reverse initiated cell death pathways including apoptosis. Tang et al. suggests that anastasis involves upregulation of pro-survival pathways to block progression of death pathways, allowing for cell rescue (Tang et al., 2018).

DNA damage is also a key feature of apoptosis, and for proper cell revival and survival, it too must be reversed. Tang et al. found that when mouse liver cells and NIH3T3 fibroblasts underwent ethanol-induced apoptosis, they exhibited AIF and EndoG release & ICAD and PARP cleavage, all which are associated with DNA breakage and degradation (Tang et al., 2018; Joza et al., 2001; Li et al., 2001; Enari et al., 1998). Yet these same cells regained function after recovery in fresh media (Tang et al., 2018), and showed a decrease in nuclear accumulation of AIF and EndoG and a decrease in cleaved- ICAD and PARP expression back to pre-apoptosis levels, indicating that DNA destruction is stopped and DNA repair is promoted in anastasis (Tang et al., 2012; Chaitanya et al., 2010). Another proposed mechanism suggesets that anastatic cells upregulate murine double minute (MDM2), a ubiquitin ligase inhibitor of p53, which represses the pro-apoptotic ability of p53, thereby preventing DNA damage (Tang et al., 2018; Tang et al., 2017; Momand et al., 1992). Expression of MDM2 also activates the X-linked

inhibitor of apoptosis protein (XIAP), ultimately terminating the death response (Tang et al., 2018; Gu et al., 2009). In addition, cell cycle arrest — crucial for DNA repair — is promoted during anastasis (Tang et al., 2018; Branzei and Foiani, 2008; Tang et al., 2017). With all said, even though cell function was restored, anastatic cells did display a high presence of micronuclei, a marker of DNA damage (Tang et al., 2018; Holland and Cleveland, 2012), signaling that remaining unrepaired DNA and resulting chromosomal aberrations are possible.

Interestingly, late stage anastasis unfolds even after cell fragmentation and formation of apoptotic bodies (Figure 1) (Tang et al., 2018; Tang et al., 2015). The mechanism behind re-fragmentation and cell structure restoration is uncertain, but surface exposure of phosphatidylserine (PS) seems to be vital for such re-fusion (Tang et al., 2018; Helming et al., 2009). In non-apoptotic, healthy cells, PS is localized to the inner plasma membrane (Tang et al., 2018). But it migrates to the outer plasma membrane during apoptosis, exposing itself as an 'eat me' signal which prompts phagocytosis (Tang et al., 2018; Arandjelovic and Ravichandran, 2015; Elliott and Ravichandran, 2016). However, in anastasis, recovering cells actively modulate PS surface-exposure; PS is exposed for a few hours, allowing for repair, but then removed to prevent phagocytosis (Tang et al., 2018; Helming et al., 2009; van Den Eijnde et al., 2001; Tang et al., 2012; Tang et al., 2015).

PROPOSED BIOMARKERS OF ANASTASIS

Evaluating the mechanism of anastasis by looking at if anastasis occurs at various hallmarks of the cell death cascade, does provide relevant insights. Transcription is highly active during anastasis allowing for necessary proteins to be synthesized to repair damage in anastatic cells (Tang et al., 2018). However, without knowing specific markers of anastasis, it will prove difficult to manipulate and assess the pathway in other cell types. To address the deficit in knowledge, Sun et al. conducted RNA sequencing (RNAseq) on untreated (control) cells, apoptotic cells, and recovering cells (at various time points of 1, 2, 3, 4, 8, or 12 hours) and observed that, compared to untreated cells, anastatic cells had 900-1,500 genes with increased abundance (> 1.5-fold) at each time point (Sun et al., 2017). Subsequent principal component analysis (PCA) revealed anastatic cells self-congregate into 2 groups based on recovery time: a cell group recovered for 1-4 hours (early stage), and a cell group recovered for 8 or 12 hours (late stage) (Sun et al., 2017). Notably, both anastasis groups are entirely distinctive from

untreated and apoptotic cells (Sun et al., 2017). Moreover, transcriptional profiling revealed early response genes are upregulated during early recovery, while late response genes are upregulated later in the recovery process (Sun et al., 2017). Further gene ontology (GO) enrichment analysis characterized the genes into categories illustrating their function, which is essential for better understanding *how* the anastasis mechanism works.

Enriched early-response genes are primarily categorized by cell cycle control and transcription level activity: “regulation of cell death,” “cellular response to stress,” “regulation of cell proliferation,” “regulation of programmed cell death,” “chromatin modification,” and “regulation of transcription,” the latter of which was the most greatly upregulated (Sun et al., 2017). Early-response genes classifications reveal that anastasis involves prompting growth-arrested cells (stuck in G1 phase) to reenter the cell cycle and begin dividing again. Furthermore, because transcription was highly upregulated, it is extremely feasible that transcription factor production is associated with progression of early-stage anastasis (Sun et al., 2017). Sun et al. further identified that such genes were upregulated in specific pathways — namely cell cycle and pro-survival cascades — including, TGFβ, MAPK, p53 and Wnt signaling (Sun et al., 2017).

By contrast, enriched late-response genes are entirely associated with posttranscriptional functions such as endocytosis, RNA transport, splicing, and ribosome biogenesis (Sun et al., 2017). Late-response clusters also show upregulation in “focal adhesion” and “actin cytoskeleton regulation” related genes, indicating possible anastatic cell migration during cell proliferation (Sun et al., 2017; Tang et al., 2018).

Moreover, recovering cells displayed prolonged upregulation of proangiogenic factors (TGFβ, Snail1, PGF/VEGFA, ANGPTLA and EphR) during both the early- and late- stages of anastasis, but especially during the latter (Sun et al., 2017; Tang et al., 2018; Tang et al., 2009). It is suspected that such factors drive angiogenesis (the growth of new blood vessels from existing ones) and vascular permeability — meliorating anastasis by increasing nutrient supply and cellular waste degradation (Tang et al., 2018; Guo et al., 2014; Simons et al., 2016).

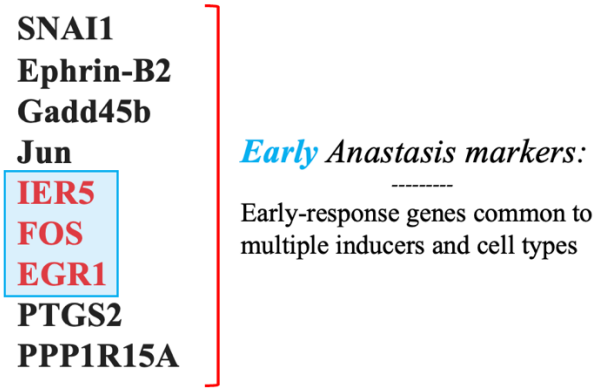

Figure 4. *A selection of some of the* ***early response genes*** *(molecular signatures) of anastasis investigated by Sun et al., 2017. These genes were upregulated in STS-induced apoptosis recovered cells. The three highlighted markers are the genes further studied in this thesis.*

The transcriptional and gene profiles associated with early-stage recovery are relatively consistent across cell lines and apoptosis inducing agents. Whilst there is some variation in the exact genes involved: for example, of the 69 genes found to be upregulated in EtOH-treated HeLa recovered anastatic cells, 44 were also enriched in STS-treated cells and 63 were enriched in EtOH-treated H4 cells, indicating there is a commonality of many response genes (Sun et al., 2017).), and the same gene categories are upregulated across the board (Sun et al., 2017).

Out of the 44 genes shown to be upregulated in STS-induced intrinsic-path apoptosis, a subset was selected by us for further investigation and three are discussed in this thesis: IER5, EGR1, and Fos (Figure 4). The roles of these genes, specifically, in regards to anastasis have not been well studied in the literature. Having said that, IER5, EGR1, and FOS and their functions have been studied in other contexts, such as apoptosis. Immediate early response 5 (IER5) regulates the cellular response to mitogenic signals (Williams et al., 1999). Further study proposes that overexpression of IER5 leads to suppression of cell growth and augmented cisplantin- or irradiation- induced apoptosis, as a result of increased caspase-3 and PARP cleavage (Yang et al., 2016; Williams et al., 1999). Early growth response-1 (EGR1) is a regulatory early-response gene, activated via the MAPK signaling pathway, that is broadly expressed across various cell types (Wang et al., 2021; Ding et al., 2021). It plays a role in multiple cellular processes including growth, differentiation, proliferation, apoptosis, and wound healing (Wang et al., 2021; Ding et al., 2021). However, the regulatory functions which activated EGR1 performs is dependent on the cell type (Wang et al., 2021; Kim et al., 2011). c-Fos (FOS) is also an early gene, which encodes a transcription factor and thus regulates the expression of

many other genes. Growth and differentiation factors or external cellular stresses activate FOS — hence it is involved in cell proliferation, differentiation, and apoptosis (Poon et al., 2000; Sheng and Greenberg, 1990; Franza et al., 1988).

Intriguingly, a portion of the early-response genes associated with anastasis were upregulated before anastasis itself had even begun — likely contributing to the quick rate of cell recovery following stress removal. mRNA transcripts of some genes which were found to be enriched within the first hour of anastasis, were already observed having increased levels of transcript expression during apoptosis compared to untreated cells (Sun et al., 2017). Upon further investigation, Sun et al. observed that even whilst apoptosis is occurring, cells position themselves for potential anastasis onset by upregulating genes which are degradation-protective and accordingly synthesize mRNA (Sun et al., 2017). Thus, soon after apoptosis induction ceases, cells immediately begin synthesizing necessary recovery proteins (Sun et al., 2017). On the contrary, if apoptosis persists, early-response mRNAs will be degraded and cells proceed to death (Sun et al., 2017).

POTENTIAL HALLMARKS OF ANASTASIS

Whilst much more research is needed to draw conclusions, plausible characteristics of anastasis have been identified based on observation in research (Figure 5) (Tang et al., 2018). These emerging functions of anastasis, carry considerable biological potential in different contexts: some in which promoting anastasis is beneficial and others in which preventing anastasis is advantageous. Reactivation of gene expression following removal of a death inducer is a hallmark of anastasis (Tang et al., 2018). Arrest of cell death executioners (caspases) and restoration of cell function are implicated in cryoprotection and tissue recovery (Tang et al., 2018), whist increased angiogenesis and cell migration are likely associated with cancer metastasis and re-emergence during chemotherapy (Tang et al., 2018; Sun et al., 2017; Salvucci and Tosato, 2012; Barquilla and Pasquale, 2015).

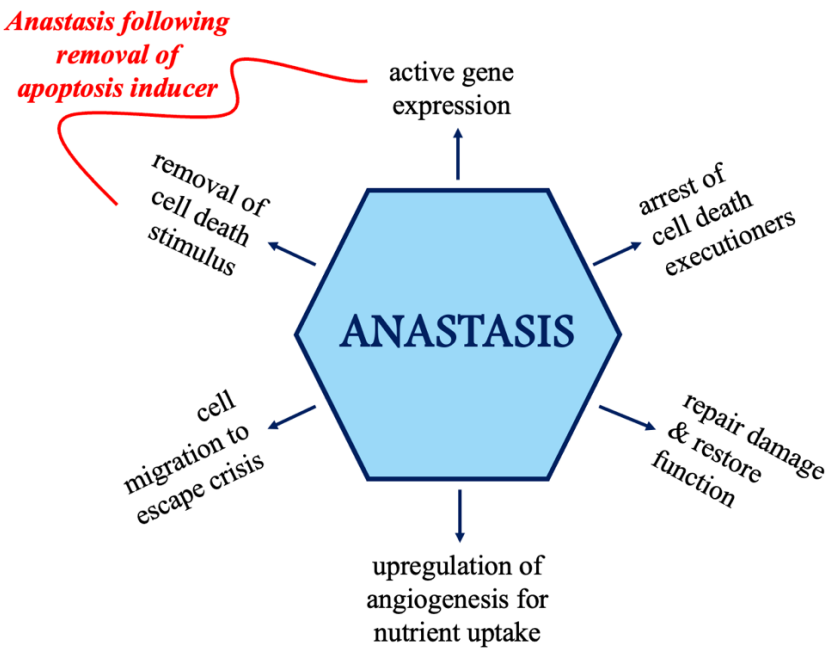

Figure 5. Hallmarks of Anastasis. Potential identifiers and features of anastasis as proposed by Tang et al. (Tang et al., 2018).

Previous Photoreceptor Studies: Rescue & Neuroprotection — Why Anastasis.

To date, anastasis in photoreceptors is a novel concept and consequently, it is not well described in current retina literature. Nonetheless, attempts and investigations of neuroprotection and PR rescue — which is the overarching goal of looking at anastasis in the context of the retina — have been, and continue to be, broadly examined in the literature. Previous efforts in achieving neuroprotection have taken many approaches; a few examples include treatment with neuroprotective agents, interference with apoptosis, and stem cell therapies (Murakami et al., 2013; Barkana and Belkin, 2004; Usategui-Martín and Fernandez-Bueno, 2021). However, each has had its respective challenges; clinical usage of inhibitory drugs is limited due to cross-involvement of treatment targets with other parts of the nervous system (Barkana and Belkin, 2004). Moreover, secondary neurodegeneration may also be caused by an excessive production of multiple substances, making targeting only one rather ineffective for overall treatment outcomes (Barkana and Belkin, 2004). Stem cells therapies do show promise as well, but defining which neurotrophic factors are critical for therapeutic effects, optimal doses, and delivery methods must all still be evaluated (Pardue et al., 2018; Usategui-Martín and Fernandez-Bueno, 2021). In addition, previous pharmacological targeting of apoptosis has been

largely unsuccessful in achieving neuroprotection (Murakami et al., 2013). Thus, retinal neuroprotection remains an active and hopefully promising area of research (Schmidt et al., 2008) and anastasis may be a new additional area of study, offering a potential target mechanism for treatment.

Present Study.

As evidenced by the literature, retinal neuroprotection is a significant area of research interest in the quest for treating various stages of neurodegenerative diseases associated with photoreceptor cell death. Previous attempts of pharmacological targeting of apoptosis have been unsuccessful in yielding neuroprotective measures (Murakami et al., 2013). Thus, inspired by cancer cells, this study aims to investigate whether anastasis is relevant to photoreceptor cells — and if so by what mechanism — to establish whether it holds any therapeutic potential in the treatment of retinal neurodegeneration.

Because anastasis has been primarily studied in cancer cells, we looked towards cancer research, which suggests that anastasis operates via upregulation of pro-survival pathways to block progression of death pathways, allowing for cell rescue (Tang et al., 2018). Based on the literature we hypothesize that an anastasis mechanism of cell recovery could work in the retina. Ergo, to investigate whether anastasis is indeed applicable to photoreceptor cells: we will perform a series of experiments which assess hallmarks of apoptosis. First, we will chemically apply stress to the photoreceptors and ensure that characteristic biochemical and morphological apoptotic markers are present. We will then examine whether upon removal of stress, the cells recover and revert to normal character by re-assessing the presence (or lack thereof) of apoptotic markers. If anastasis appears to be relevant to photoreceptors, we would expect to see a reduction of previously present signs of apoptosis. Moreover, if anastasis is shown to be applicable to the retina, the mechanism of — namely *how* — cell recovery occurs after stress removal must then be determined.

Accordingly, this thesis is a small portion of the research and experiments performed as part of a larger project conducted by the Zacks lab to critically investigate anastasis in photoreceptor cells.

Methods

661W Mouse Retinal Photoreceptors & Cell Culture.

The 661W cone photoreceptor (PR) cell line, provided by Dr. Muayyad Al-Ubaidi (University of Oklahoma Health Sciences Center, Oklahoma City, OK, USA), was used for *in vitro* experiments. This mouse-derived cell line expresses multiple markers of cone photoreceptor cells and is broadly used as a model for studying macular degeneration, a neurodegenerative disease (Sayyad et al., 2017; Wheway et al., 2019). The cells were maintained and cultured in a Dulbecco's Modified Eagle Medium (DMEM) (Gibco, cat# 11885-084), which also contained 10% FBS (Corning, cat# 35-015-CV) and 1% Penicillin-Streptomycin (Gibco, cat# 15140122), 32 mM putrescine, 40 μL/L β-mercaptoethanol, 40 μM hydrocortisone 21-hemisuccinate, and 40 μM progesterone. Cells were split and cultured as needed and were incubated at 37°C in a humidified atmosphere of 5% CO_2 and 95% air.

Drug Treatment.

Apoptosis was initiated in 661W cells using staurosporine (STS) (ALX-380-014-M001, Enzo) a known apoptosis inducer and potent cell-permeable protein kinase inhibitor (Anon PubChem, n.d.). Staurosporine binds to the ATP binding site and inhibits various protein kinases (PKC, CDK1/cyclin B, CDK2/cyclin A, CDK4/cyclin D, CDK5/p25, GSK-3β, and Pim-1) and topoisomerase II, resulting in apoptosis and cytotoxicity (Anon PubChem, n.d.). Staurosporine has been shown to trigger apoptosis primarily via the intrinsic signaling pathway (Malsy et al., 2019). Drug treatment was prepared as a stock solution with 1mM staurosporine in DMSO (Dimethyl sulfoxide), and then further diluted. Concentrations of 0.05, 0.1, 0.2, 0.3, 0.4 (μM) were assessed using MTT and Crystal Violet assays for efficacy in inducing apoptosis, and 0.05 μM was decided upon as the treatment concentration.

Once an appropriate concentration was determined, photoreceptor cells were treated as follows, also schematized in Figure 6: Control cells were placed in normal DMEM culture medium. Treatment cells were treated with 0.05 μM staurosporine for 15 hours and then collected. Recovery (Anastasis) cells were treated with 0.05 μM staurosporine for 15 hours. At the 15-hour time point, the drug treatment was removed, cells were washed with PBS, and fresh DMEM was added. Recovery cell samples were collected at two different timepoints: 24 hours

after media change and 48 hours after media change. Endpoint cells were treated with staurosporine indefinitely until they were collected at the same time points as the Recovery cells.

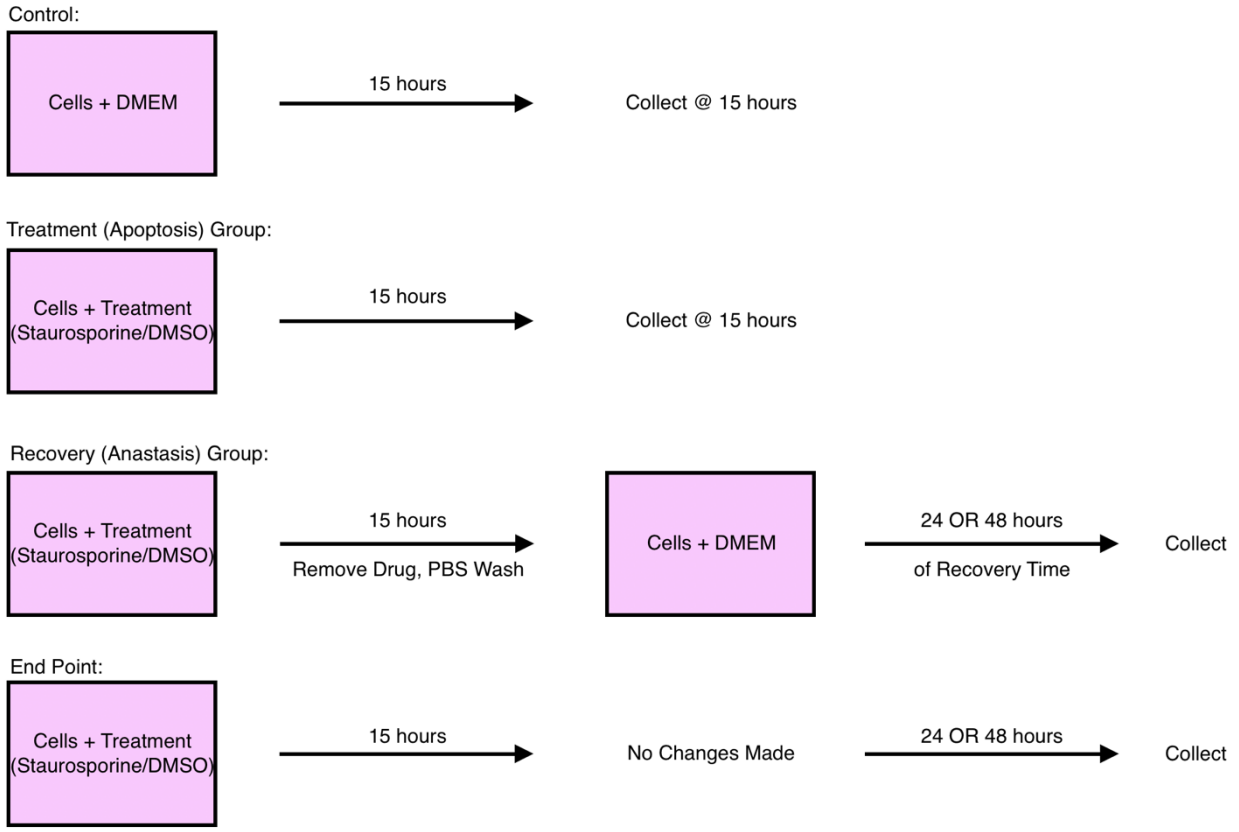

Figure 6. Experimental treatment methods for Control, Treatment, Recovery, and End Point groups. Collection of the Control and Treatment groups occurred at 15hrs, following treatment. Recovery group had the drug removed and replaced with fresh media at 15hrs, and collection occurred at either 24 or 48 hours after media change. End Point group was treated and subsequently incubated with no changes made, and then collected at the same time as the Recovery group.

MTT Assay.

After collection, cells were washed with PBS. Subsequently, the MTT solution was added to each of the wells containing cells. MTT solution was prepared with the reagent Thiazolyl blue tetrazolium bromide (Sigma – M5655-100MG) (25mg) into PBS (50 mL). Cell plates were then lidded and covered with foil and incubated at 37° for 3 hours. Dark-blue formazan crystals formed, based on mitochondrial dehydrogenase enzyme activity, and were retained only within viable cells. The resulting crystals were dissolved in isopropanol and the absorbance of the crystal solution was measured at 540 nm using a calorimeter, to evaluate mitochondrial activity and thus indirectly assess cell viability. MTT was used to assess cell

viability in order to determine if the staurosporine drug treatment concentration induced apoptosis or not. (Methods based on lab protocol).

Crystal Violet: Assay & Imaging.

Crystal Violet solution (0.5% Crystal Violet (Sigma C6158 – 50g) in 20% methanol) was added to cells after washing them with PBS. Cells were then incubated for 15 minutes, allowing crystals to form, and subsequently rinsed with water. To view cell morphology, EVOS was used to image and photograph the wells. The crystals were then resuspended in methanol and the absorbance of the resulting solution was measured at 595 nm to determine if there is cell proliferation based on the detection of adherent cells (Feoktistova et al., 2016). (Methods based on lab protocol).

RNA Isolation, cDNA Preparation, & qRT-PCR.

Total RNA was extracted from retinal tissue using the RNeasy® Plus Micro kit (Qiagen Sciences, cat# 74034), according to the manufacturer's Quick-Start protocol. Samples were prepared and RNA concentration and quality were evaluated using the NanoDrop® Spectrophotometer. Following this, complementary DNA (cDNA) was synthesized the total RNA using the High-Capacity cDNA Reverse Transcription Kit (Thermo Fisher, cat# 4368814) using the manufacturer's recommended protocol. Real-Time Quantitative Reverse Transcription PCR (qRT-PCR) was performed using CFX384 Touch (Bio-Rad), utilizing the specified primer sequences:

Fast SYBRTM Green Master Mix (Applied Biosystems, cat# 4385612).

Pum1 (Forward: ACAGCCTGCCAACACGTCCTTG, Reverse: CCACTGCCAGTGTTGGAGTTTG)

Pum1 was used as a housekeeping gene (control) to normalize the different experimental RNA samples. The total reaction volume used for qRT-PCR was 10µL. Relative gene expression levels of IER5, EGR1, and FOS were assessed via the ΔΔCt method of qPCR assay data analysis. The forward and reverse RNA sequences of IER5, EGR1, and FOS – the genes of interest (Anastasis markers) – used were:

IER5 (Forward: ACGCGTCACCAGGTCTTTTC, Reverse: TGTAGGCGGGATCAGGTCTT)

EGR1 (Forward: TTCAATCCTCAAGGGGAGCCG, Reverse: CGATGTCAGAAAAGGACTCTGTGG)

FOS (Forward: GTGAAGACCGTGTCAGGAGG, AGTTGATCTGTCTCCGCTTGG)

The PCR cycling conditions consisted of an initial denaturation at 25°C for 10 minutes, followed by 37°C for 2 hours, and then 85°C for 5 minutes.

Western Blot.

During collection, cells were first harvested and scraped from plates, and total protein was then extracted from cells via cell lysis. RIPA buffer (Sigma, cat# R0278) containing phosphatase and protease inhibitors (Thermo Scientific, cat # A32957 and A32955, respectively) was used to lyse the cells and retinal tissues. Protein concentration was assayed using the RC DC™ Protein Assay Kit (Bio-Rad, cat# 5000120). Subsequently, 20 µg of protein was loaded into each well. Using a 4% to 15% SDS-PAGE (Mini-PROTEAN TGX; Bio-Rad, cat# 4561086), proteins were separated and thereafter transferred to a polyvinylidene fluoride membrane (PVDF; Bio-Rad, cat# 1620177). The membranes were then blocked with 5% bovine serum albumin (BSA; Sigma, cat# A7906) in tris-buffered saline (TBS; Bio-Rad, cat# 1706435), and incubated overnight, at 4ºC, with the primary antibody. The following primary antibodies were used: anti-mouse CHOP (1:1000; Cell Signaling Technologies, cat# 2895); anti-rabbit pIRE1 (1:1000; Novus Biologicals, cat# NB100-2323SS; anti-mouse BiP/Grp78 (1:1000; BD Biosciences, cat# 610979); anti-mouse mono-and poly-ubiquitinated conjugates (1:1000; Enzo Life science, cat# BML-PW8810); anti-mouse caspase 3 (1:1000; Novus Biologicals, NB100-56113); anti-mouse HIF1 (1:1000; R&D systems, cat# MAB1536), anti-rabbit FUNDC1 (1:1000; Novus Biologicals, cat# NBP1-81063), anti-rabbit PINK1 (1:1000; Novus Biologicals, cat# NB100-493), anti-rabbit PARKIN (1:1000; Novus Biologicals, cat# NBP2-67017), anti-mouse PGC-1 (1:500; SantaCruz, cat# sc-517380) and anti-mouse NRF2 (1:500; SantaCruz, cat# sc-365949). Membranes were washed three times with a solution of 0.1% Tween-20 in TBS (TBS-T), followed by incubation with the appropriate secondary antibody for 1 hour. The secondary antibody used was either anti-rabbit IgG, HRP linked; (1:5000; Cell Signaling Technologies, cat# 7074S), or anti-Mouse IgG (1:8000; GE healthcare Lifesciences, cat#

NA931). Gel loading controls consisted of anti-mouse- β-actin antibodies, since β-actin is expressed in all eukaryotic cells and is unaffected by most cellular treatments (Zhang et al., 2012). Proteins were quantified using single bands located within the pertinent molecular-weight region of each respective protein which was studied. Lastly, membranes were developed using the SuperSignalTM West Pico PLUS Chemiluminescent Substrate (Thermo Scientific, cat# 34580,) and the resulting blots were imaged using the cSeries Capture Software (c500; Azure Biosystems). Western blots were quantified using ImageJ2 software.

Statistical Analysis Methods.

Data and results are represented as the mean ± standard error of the mean (SEM). Statistical analysis of all experimental data was performed using GraphPad Prism 10.1.0 statistical software (GraphPad). For MTT and Crystal Violet assays for concentration kinetics, Western Blot analysis of PARP, and RT-PCR experiments: One-way ANOVA (Analysis of variance) with repeated measures (along with the Brown–Forsythe test), succeeded by Tukey's Multiple Comparisons, was used to complete statistical analysis. For Crystal Violet assays for 24- and 48-hours recovery: 2-way ANOVA and post hoc Tukey's Multiple Comparisons test were used to complete statistical analysis. Statistical significance for all tests completed is denoted in the figures by asterisks (*): *$p < 0.05$; **$p < 0.01$; ***$p < 0.001$; ****$p < 0.0001$. ns indicates no statistical significance.

Results

MTT: Cell Viability Assay for Concentration Kinetics.

Mouse photoreceptors were treated with staurosporine to stress the cells and trigger the cell death pathway. Whilst previous studies have shown that staurosporine is able to induce apoptosis, the exact concentration required to induce the pathway in 661W mouse photoreceptors has not been established (Malsy et al., 2019). To determine the optimal concentration for treatment to induce apoptosis, but not completely kill all of the cells, MTT was performed, and cell viability was assessed. Figure 7 compares the amount (in percentage) of viable cells treated with different concentrations of staurosporine, along with the control group which was only included cells with fresh DMEM media. As shown in the figure, all treatments resulted in a decrease in the amount (%) of viable cells. Thus, it was confirmed that staurosporine successfully induced apoptosis.

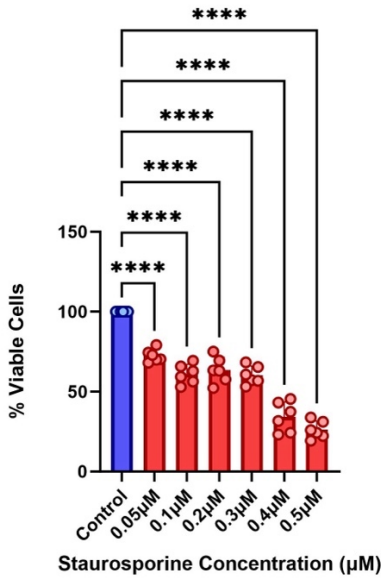

Figure 7. Decrease in the percent (%) of viable cells after 15-hour treatment with staurosporine. Percent of viable cells were normalized to the control (DMEM only) of 100% (N=6). Treatment with all concentrations of staurosporine significantly reduced cell viability. Data are shown as means ± SEM, along with individual replicate points. One-way ANOVA and Tukey's Multiple Comparisons test were used for statistical analysis. Significance is denoted by **** , for $p < 0.0001$.

The results also indicate that treatment concentrations of 0.4µM and 0.5µM resulted in the greatest decrease, with an average of only 34.2% and 25.15% of cells being viable and therefore 65.8% and 73.85% cell toxicity, respectively (Figure 7). However, these concentrations killed too many cells. It was decided that approximately 30-40% cell toxicity was the amount

necessary for experiments, and treatment with 0.05µM resulted in a mean 72.5% viable cells and 27.5% cell toxicity, compared to control cells with 100% cell viability (Figure 7). This was close to the desired cell toxicity. Because it was the minimum concentration which induced sufficient cell toxicity, 0.05µM was selected as the treatment concentration to be used in proceeding experiments.

Crystal Violet Staining: Cell Proliferation Assay for Concentration Kinetics.

Crystal Violet assay was the second measure used to ensure that apoptosis was induced in photoreceptor cells and that 0.05µM was an adequate concentration for treatment. Because cell death causes adherent cells to detach from cell culture plates, this measure was used to indirectly quantify cell death and establish the variability in cell proliferation following application of death inducing agents (Feoktistova et al., 2016). Attached cells, which can proliferate, are characteristic of healthy cells.

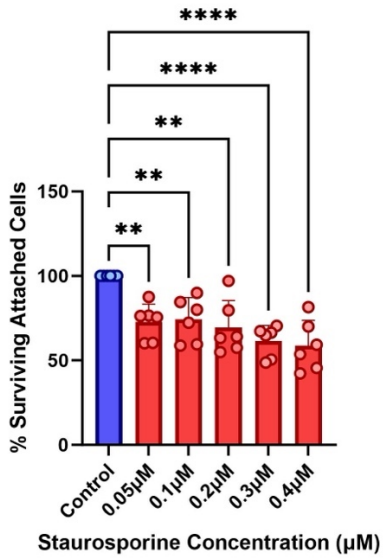

Figure 8. Decrease in percent (%) of surviving cells and cell proliferation after 15-hour treatment with staurosporine and DMEM only control. Percent of attached cells were normalized to the control (DMEM only) of 100% (N = 6). Treatment with all concentrations of staurosporine (0.05, 0.1, 0.2, 0.3, 0.4 µM) significantly reduced the amount of surviving attached cells. Data are shown as means ± SEM, along with individual replicate points. One-way ANOVA and Tukey's Multiple Comparisons test were used for statistical analysis. Significance is denoted by **, for $p < 0.01$ and ****, for $p < 0.0001$.

All staurosporine treatment concentrations exhibited a significant decline in the percentage of attached cells, and therefore a decline in cell proliferation as well. A drug concentration of 0.05µM resulted in a mean 72.74% ($p < 0.01$) of attached cells and a 26.26%

decrease in proliferation, compared to control cells with 100% surviving attached cells (Figure 8). It was decided that approximately a 30% decrease in cell proliferation was required for experimental toxicity treatments, so 0.05µM was again deemed sufficient and selected for subsequent treatment concentrations.

Morphology.

Apoptotic cells have unmistakable and visible structural changes which are caused and mediated by caspase activation (Green and Llambi, 2015). Thus, morphological evaluation served as another method to determine whether apoptosis occurred, as well as to monitor the physical health of recovering cells. Crystal violet staining followed by imaging was used to detect apoptosis. Changes in photoreceptor cell morphology occurred after 15 hours of staurosporine (0.05µM) treatment and again after 48 hours of recovery in fresh DMEM media (Figure 9).

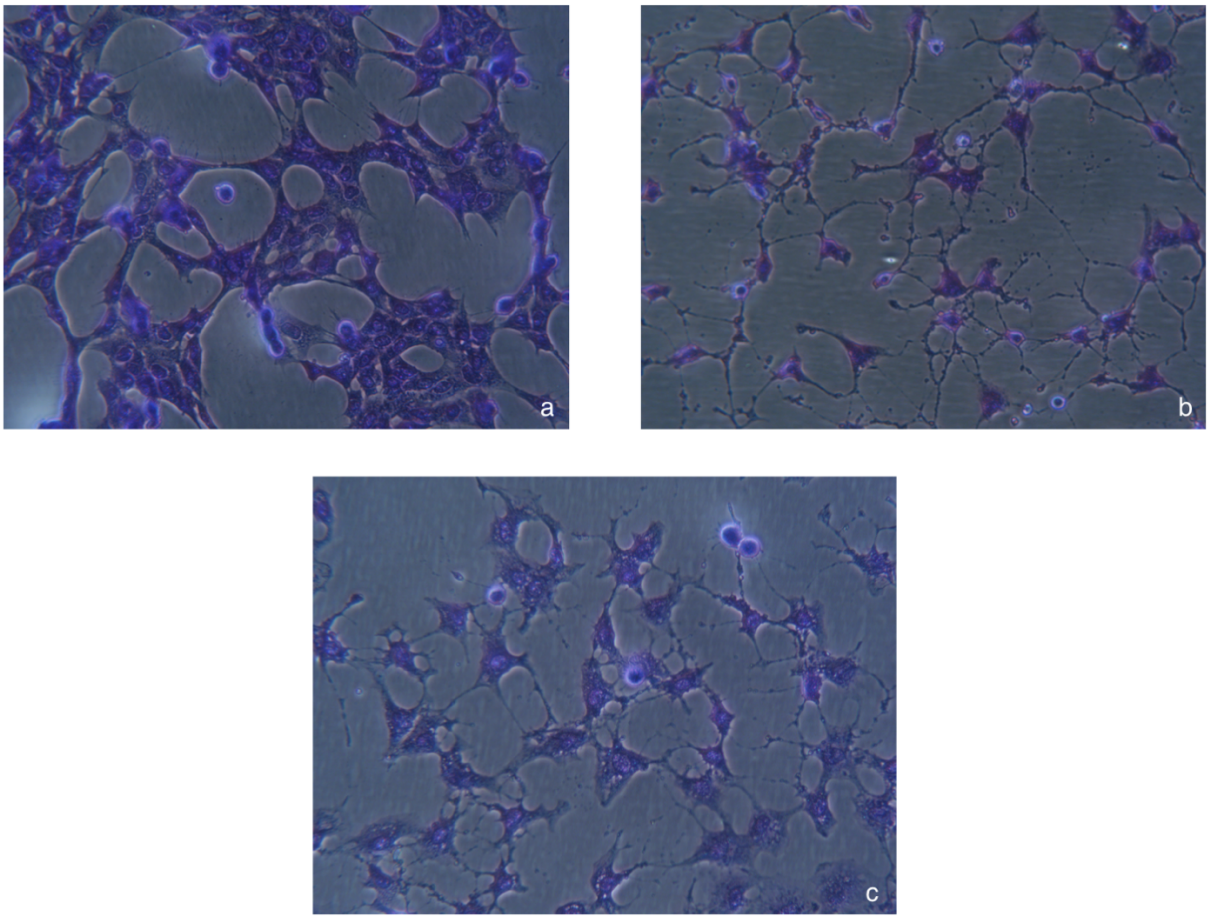

Figure 9, a-c. EVOS imaging of cells after Crystal Violet staining*: Control (a), Treatment with staurosporine 0.05µM for 15hrs (b), and Anastasis group with 48hrs recovery time (c).*

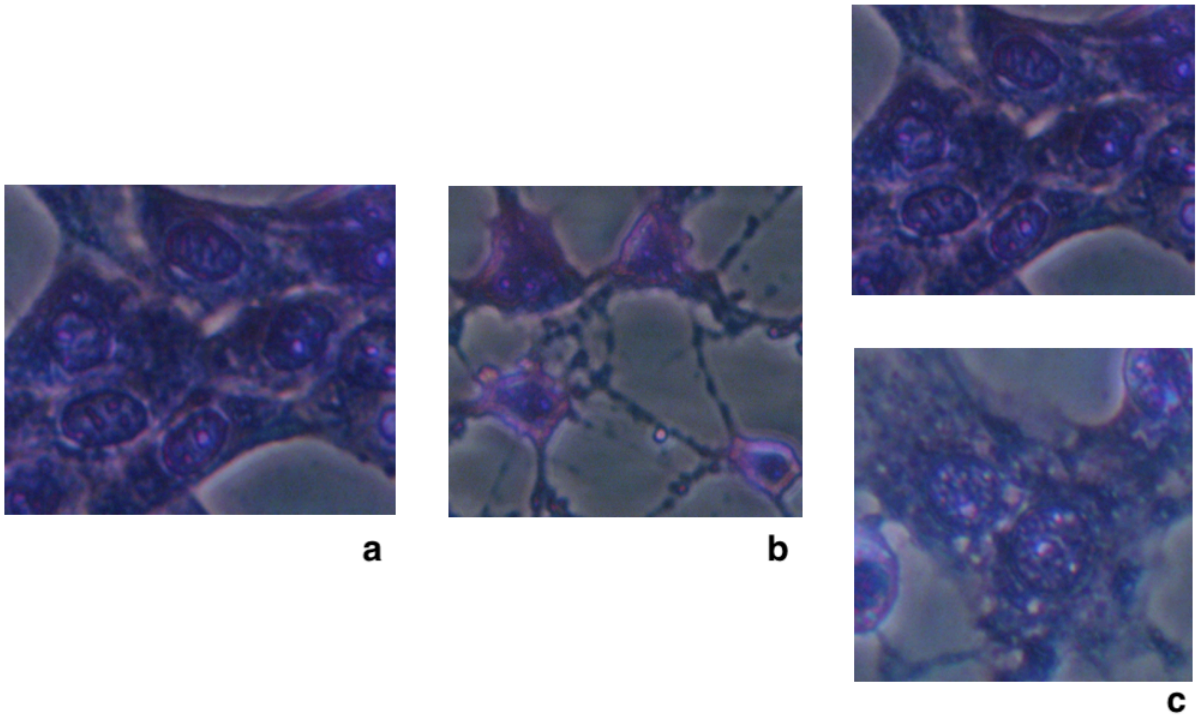

Figure 10, a-c. *Close up selections of some photoreceptor cells captured by EVOS imaging of cells after Crystal Violet staining, to identify changes in morphology: Control (a), Treatment with staurosporine 0.05μM for 15hrs (b), and Anastasis group with 48hrs recovery time (c).*

The violet regions represent the photoreceptor cells. Control cells (Figure 9a) showed a normal healthy morphology, as cells are elongated and circular plasma membranes are evident. Upon closer inspection, many of the healthy cells connected with each other, indicating proper cell-cell communication (Khalili and Ahmad, 2015; Alberts et al., 2002). Following treatment with 0.05μM staurosporine, photoreceptor cells exhibited morphological changes (Figure 9b). A decrease in the violet stained regions was observed: many cells were no longer proliferating and were therefore not stained. Some cells fully reached the end of apoptosis and died, but many cells were on the path towards apoptosis as indicated by their altered morphology. The stained treatment cells showed a skeletal, shrunken structure instead of a rounded shape like the control cells (Figure 10a,b). Treatment cells also appeared misshapen with blebbed membranes as opposed to ones which are clear and rounded. Cellular contents were less visible in treatment cells (Figure 10b). Accordingly, imaging findings further confirmed that apoptosis was successfully induced by staurosporine in 661W photoreceptors, evidenced by morphological changes characteristic of apoptotic cells.

Anastasis/recovery group showed increased crystal violet staining and cell proliferation compared to treatment cells (Figure 9b,c). Connections between some cells also seemed to re-form. Cell membranes also recovered a clearly visible rounded shape and no membrane blebbing was visible (Figure 10c). Cellular contents were also evidently present in anastasis/recovery cells. The morphology of anastasis group cells also appeared more similar to control cells than treatment cells, even though apoptosis had been triggered by staurorporine in former group as well. Indeed, cells in the anastasis/recovery actually began showing signs of recovery to healthy morphology as early as 6 hours after staurosporine was removed and replaced with fresh DMEM. Anastasis group photoreceptors showed a more normal morphology after recovery, but whether or not the cells functioned normally (in the manner of healthy cells), remained to be investigated.

Crystal Violet Assay of Cells following 24 hours of Recovery.

To verify if the morphological changes after recovery were actually indicative of cell health, cell proliferation was evaluated for anastasis (recovery) group cells which were exposed to STS for 15 hours and then incubated in fresh DMEM for 24 hours, to recover. Crystal violet assay was performed to address if photoreceptor cells were recovering functions of healthy cells after the stressor (staurosporine) was removed. Statistical analyses revealed that there was no significant difference in the percent of surviving attached cells between anastasis cells and treatment cells at any of the tested staurosporine concentrations (Figure 11, a-b). These results indicated that there was no cell proliferation found in the anastasis group cells, and that the first 24 hours in fresh media was a recovery period.

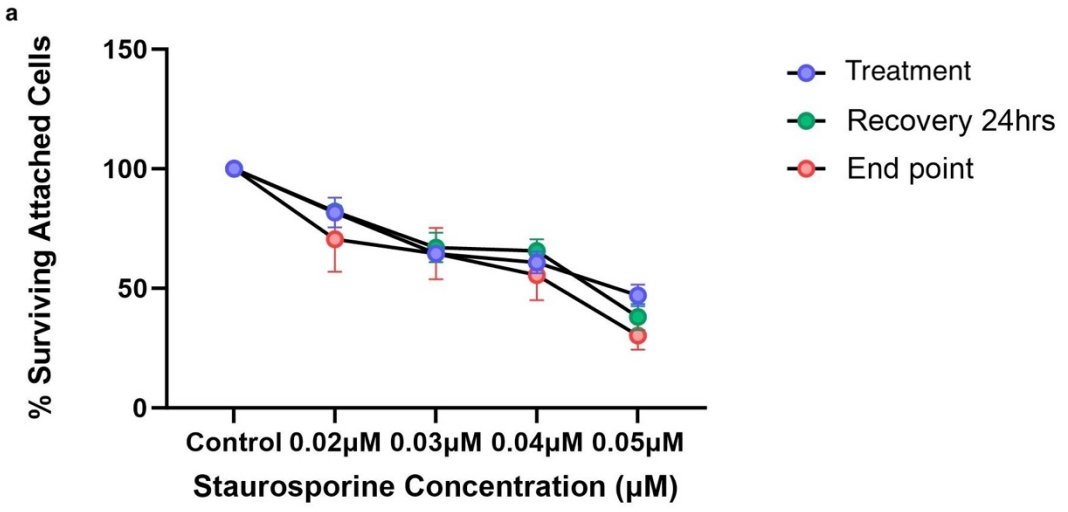

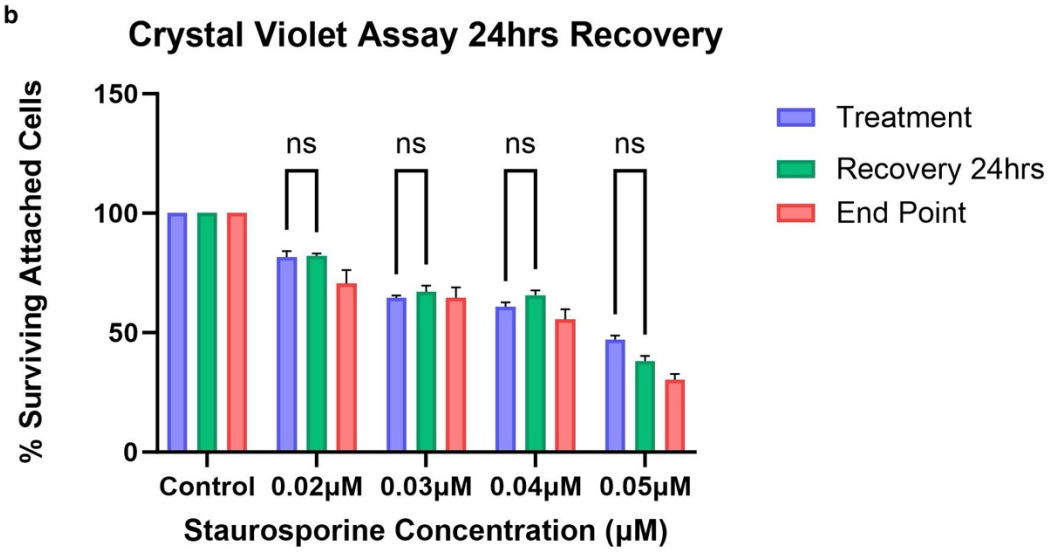

Figure 11, a-b. 24 hours of recovery time (following 15-hour treatment with staurosporine) did not result in any significant change in the percent (%) of surviving cells, compared to treatment cells without recovery. Percent of attached cells were normalized to the control (DMEM only) of 100% (N = 6). All cell groups in Control measure were treated with only DMEM. Endpoint cells in the concentration groups were treated with drug for 35 hours. They did not receive a fresh media change and served as second control measure. Data are shown as means ± SEM. 2-way ANOVA and Tukey's test for multiple comparisons were used for statistical analysis. Lack of significance is denoted by ns (not statistically significant).

Crystal Violet Assay of Cells following 48 hours of Recovery.

Because no proliferation was found at the 24-hour recovery timepoint, 48 hours of recovery was thence investigated. Crystal violet staining was conducted at this timepoint and increased staining in the photoreceptor cells of anastasis recovery cells as compared to treatment group photoreceptors was observed in all tested drug concentrations. The percent of surviving attached cells indicate the quantity of cells and it can be inferred that after 48 hours of recovery, photoreceptors were proliferating (dividing). Accordingly, the level of cell proliferation in 48-hour recovery cells trended above that for each of the respective concentration matched treatment cells (Figure 12a). Significant cell proliferation was found following recovery after treatment with: 0.02µM ($p < 0.05$), 0.03µM ($p < 0.0001$), 0.04µM ($p < 0.0001$), 0.05µM ($p < 0.001$) (Figure 12b). The findings support the conclusion that 48-hour recovery resulted in the increased presence of healthy cells and recovery of some characteristic normal cell functions, namely ability for cell division.

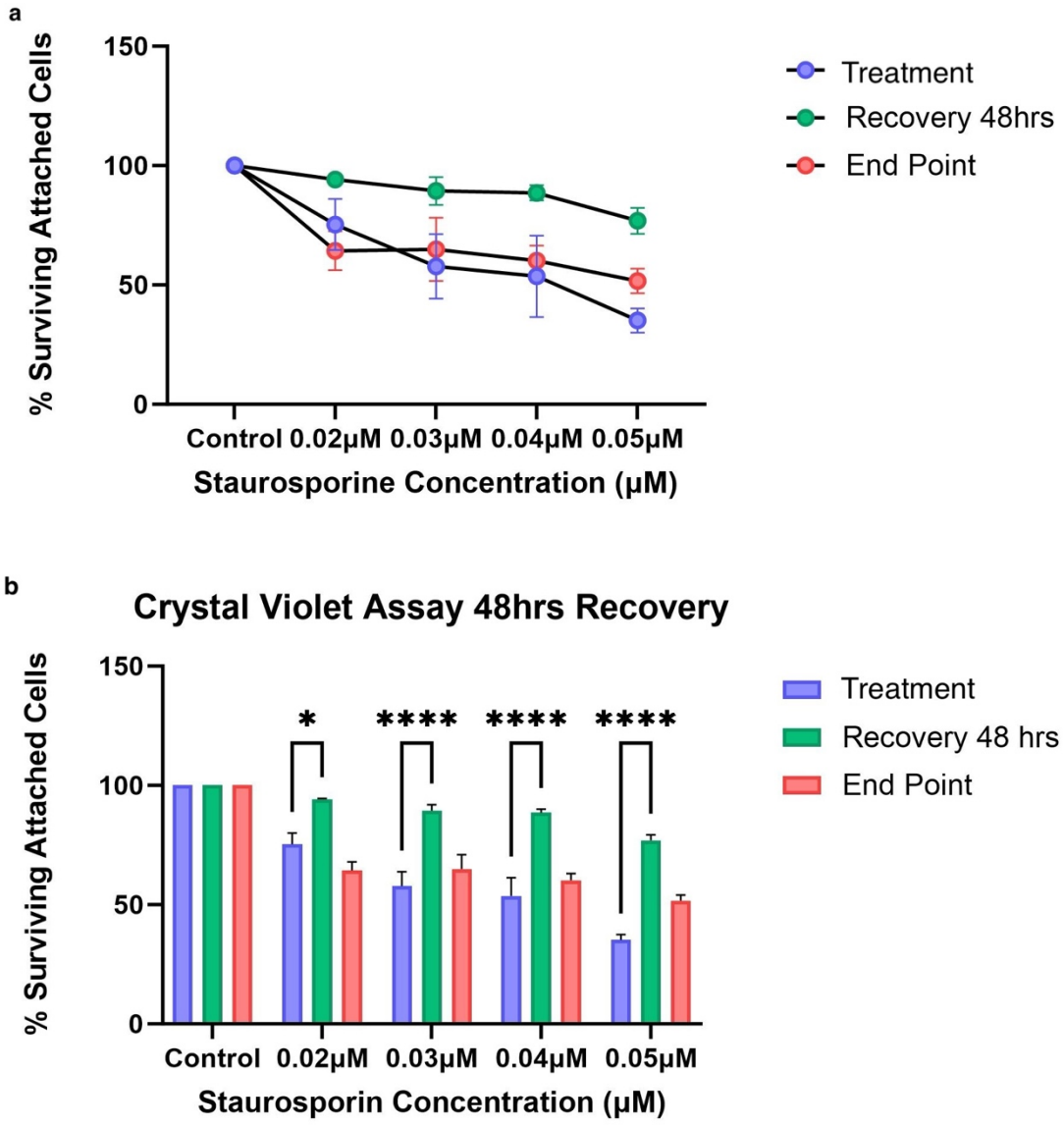

Figure 12, a-b. 48 hours of recovery time (following 15-hour treatment with staurosporine) resulted in a significant increase in the percent (%) of surviving cells and cell proliferation, compared to treatment cells without recovery. Percent of attached cells were normalized to the control (DMEM only) of 100% (N = 6). ***(a) Data presented as a line graph across staurosporine treatment concentrations. (b) Data presented as a bar graph, illustrating comparisons between cell proliferation of Treatment cells and Recovery cells.*** All cell groups in Control measure were treated with only DMEM. Endpoint cells in the concentration groups were treated with drug for 35 hours. They did not receive a fresh media change and served as second control measure. Data are shown as means ± SEM. 2-way ANOVA and Tukey's test for multiple comparisons were used for statistical analysis. Significance is denoted by *, for $p < 0.05$ and ****, for $p < 0.0001$.

Western Blot & Changes in PARP Expression after 48 hours of Recovery.

To further confirm if cell function was recovered after removal of the cellular stressor (*0.05µM staurosporine for 15hrs)*, immunoblotting was used to detect the presence of PARP protein and cleaved-PARP protein in both treatment-only and recovery+treatment photoreceptor cells (Figure 13a). A thicker and darker band, representing cleaved-PARP protein expression, was visible in the blot for treatment-only and recovery+treatment cells. Increased cleaved-PARP levels has been associated with a greater presence of apoptosis (Chaitanya et al., 2010; Ward et al., 2008) (Figure 13).

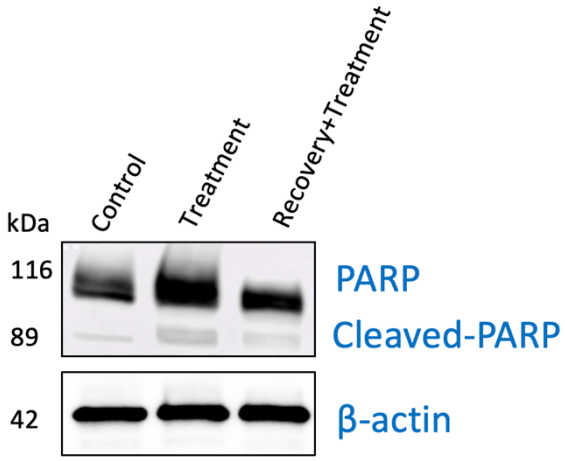

Figure 13. Western blot analysis of* PARP *and cleaved*-PARP *protein levels in Control, Treatment *(0.05µM staurosporine, 15hrs)****, and Recovery+Treatment cells*** *(0.05µM staurosporine 15hrs and recovery 48hrs)****.*** Cells treated with DMEM only were used as controls. β-actin served as loading controls.

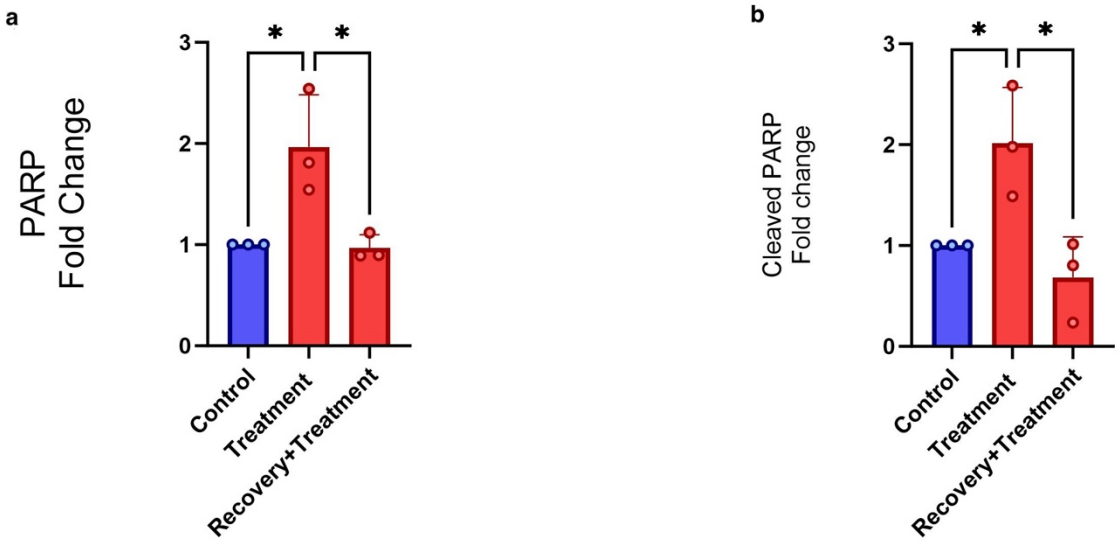

Figure 14, a-b. 48 hours of recovery time in DMEM following 15 hours of staurosporine treatment significantly reduced PARP and Cleaved-PARP expression in 661W mouse photoreceptor cells.

(a) Quantification of relative PARP protein levels (fold change) based on densitometry of the Western blot (N = 3). Data are shown as means ± SEM, along with individual replicate points. One-way ANOVA and Tukey's Multiple Comparisons test were used for statistical analysis. Significance is denoted by *, for $p < 0.05$. ***(b) Quantification of relative Cleaved-PARP protein levels (fold change) based on densitometry of the Western blot (N = 3).*** Data are shown as means ± SEM, along with individual replicate points. One-way ANOVA and Tukey's Multiple Comparisons test were used for statistical analysis. Significance is denoted by *, for $p < 0.05$.

PARP expression in control DMEM only photoreceptor cells was assessed to establish a baseline of expected PARP levels in healthy cells (Figure 14a). The fold change in PARP protein levels was normalized to the control (Fold change = 1). Treatment-only cells showed a statistically significant increase in PARP protein levels (mean Fold change = 1.966, $p < 0.05$) in comparison to both the control and the recovery+treatment cells. Recovery+treatment cells (mean Fold change = 0.968) had a significant difference in PARP-1 protein expression when compared to Treatment-only cells ($p < 0.05$), but not compared to control ($p = 0.912$, ns) (Figure 14a). Significant increase in protein levels of PARP-1 in treatment-only cells (represented by a mean fold change value larger than control=1 (1.977 > 1)), compared to control and recovery, suggested presence of cell stress increased PARP-1 levels. Healthy cells (control) showed lower levels of PARP-1 protein. Recovery+treatment cells (48hrs in fresh DMEM) showed reduced PARP-1 protein expression compared to treatment-only cells, the latter of which were representative of apoptotic cells. Indeed, recovery group did not exhibit a significant change in PARP-1 levels compared to healthy control cells, which were neither stressed nor death induced.

Low baseline expression of cleaved-PARP, indicative of healthy cells, was detected in control DMEM only photoreceptor cells and the fold change in cleaved-PARP levels was normalized to the control (Fold change = 1) (Figure 14b). Treatment-only cells displayed a significant increase in cleaved-PARP-1 protein expression (mean Fold change = 2.017, $p < 0.05$) compared to control and recovery+treatment cells. The significantly greater levels in treatment-only cells compared to both the control and recovery cells indicated that apoptotic stress was associated with increased cleaved-PARP-1 expression. Recovery+treatment cells (mean Fold change = 0.689) were found to have significantly decreased cleaved-PARP-1 protein levels compared to treatment only cells ($p < 0.05$), but not compared to control cells (Figure 14b). Healthy cells exhibited significantly lower levels of cleaved-PARP-1 protein in comparison to treatment-only cells, but no significant difference was found between control and

recovery+treatment cells (Figure 14b). These results indicate that recovery+treatment cells, representative of anastatic cells, show cleaved-PARP-1 expected of healthy cells.

These findings support the conclusion that after 48 hours of recovery, photoreceptor cells which were stressed no longer show PARP-1 nor cleaved-PARP-1 protein levels expected of apoptotic cells. The results reveal that cells in recovery may demonstrate principals of anastasis.

Real-Time Polymerase Chain Reaction (RT-PCR) of IER5, EGR1, & FOS after 48 hours of Recovery.

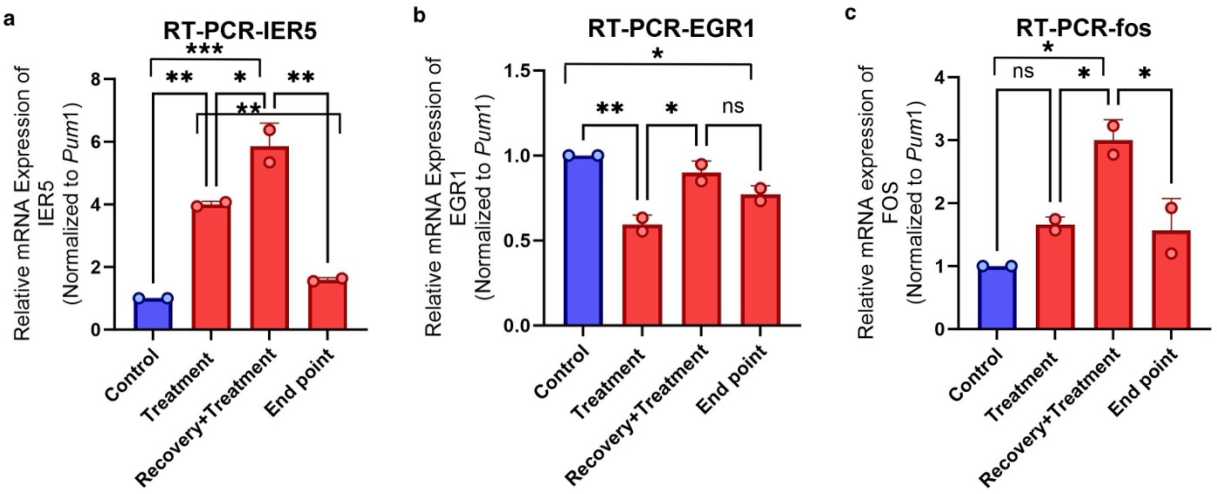

Figure 15, a-c. Relative mRNA expression levels of anastasis markers: IER5 (a), EGR1 (b), and FOS (c) in 661W mouse photoreceptor cells, normalized to Pum1, used as the housekeeping gene (N = 2). Cells treated with DMEM only were used as controls. Endpoint cells were treated with STS for 35 hours (continuously until collection). Data are shown as means ± SEM, along with individual replicate points. One-way ANOVA and Tukey's Multiple Comparisons test were used for statistical analysis. Significance is denoted by *, for $p < 0.05$; **, for $p < 0.01$. *** ; for $p < 0.001$ and ns (no significance).

A gene expression profile associated with anastasis has been described (Sun et al.). We used qRT-PCR to assess if we could detect a similar gene expression profile in our cells. mRNA expression of IER5 was significantly increased in treatment-only and recovery+treatment group PRs in comparison to untreated control cells ($p < 0.01$ and $p < 0.001$, respectively). mRNA transcript level was also significantly greater in recovery+treatment cells compared to treatment-only cells ($p < 0.05$). (Mean relative mRNA expression of IER5 was: control = 1, treatment-only = 4.003, recovery+treatment = 5.860).

Treatment-only cells, representative of apoptotic cells, showed a significant decrease in EGR1 transcript expression compared to control ($p < 0.01$) and recovery+treatment ($p < 0.05$) cells. There was no significant difference found between the mRNA expression in untreated

control cells and recovery+treatment cells (ns, p = 0.3326). (Mean relative mRNA expression of EGR1 was: control = 1, treatment-only = 0.594, recovery+treatment = 0.899).

Recovery+treatment group cells showed a significantly greater expression of FOS mRNA compared to all other experimental groups ($p < 0.05$). On the other hand, there was no significant difference in FOS transcript expression found between control and treatment-only cells. (Mean relative mRNA expression of Fos was: control = 1, treatment-only = 1.657, recovery+treatment = 3.000).

Discussion

In this study we demonstrated that anastasis is a viable and applicable mechanism in 661W mouse photoreceptor cells. In the experiments performed, after treatment with staurosporine, cells began showing signs of death/apoptosis and then subsequently recovered after stress removal.

Until now, anastasis has not been studied in ophthalmologic nor retinal research and so present findings are compared to cancer research. As observed in many studies, apoptosis is markedly characterized by certain distinct morphological changes. Crystal violet staining illustrated apoptotic features — such as condensed and shrunken cells, deformed shape, and membrane blebbing — occurred after treatment, confirming apoptosis induction. After 48 hours of recovery in fresh media with the stress removed, apoptotic cells no longer showed a morphological profile of apoptosis. Instead rounded, integrate membranes with clearly visible cellular contents were observed, similar to what was viewed in control (untreated, healthy) cells. Morphological recovery and cell reformation are fundamental physical signs of anastasis (Tang et al., 2009; Tang et al., 2012), and these results indicate anastasis occurs in photoreceptors. It is to be noted though, that we allowed PRs to recover for 48 hours before assessing morphology, whereas other studies witnessed structural changes beginning at 24 hours after apoptotic stimuli were removed (Tang et al., 2009).

Furthermore, biochemical evidence representative of anastasis was also observed in the crystal violet assays we performed. After being allowed to recover for 48 hours in fresh media, previously-apoptotic (now recovered) photoreceptor cells showed a significantly increased amount of viable and attached cells compared to the amount shown by apoptotic cells. This finding indicates that when apoptotic stress is removed, cell proliferation increases, which is an archetypal characteristic of anastatic cells as described in previous studies (Tang et al., 2009; Tang et al., 2012). Whilst our results at 48-hours do suggest anastasis mediated proliferation occurs, the observed time frame varies in comparison to other studies. Notably, no significant difference in the amount of healthy, attached cells between apoptotic cells and cell which had 24 hours of recovery in fresh DMEM were found in our 24-hour crystal violet assay results. Based on this, there was no cell proliferation observed, in the 24-hour recovery group cells, to which we concluded that 24 hours in fresh media was not enough time to regain dividing functions of healthy cells. Again, the fact that prior studies used cancer cells and/or different apoptosis

inducers must be considered, but time frame differences were noted. Tang et al. found that jasplakinolide-induced HeLa cells showed cell proliferation within 24 hours after the stress inducer was removed and even more increased proliferation by the 48-hour mark (Tang et al., 2009). Similarly, in EtOH treated HeLa cells, the numbers of cells increased during the first 11 hours of recovery, remained stable for a period, and then increased again at around 30 hours of total recovery time (Sun et al., 2017). Both these findings differ from our observations because no signs of increased cell proliferation, that could be associated with anastasis, were observed in photoreceptors recovered within 24 hours. However, our results indicated that the first 24 hours was a necessary recovery period — in which anastasis was underway — before photoreceptors began proliferating, as observed by the 48-hour recovery mark. Additionally, Sun et al. observed two stages (early and late) of anastasis (Sun et al., 2017), which we did not in our experiments. Whether two phases exist in photoreceptors will need further investigation of time points, especially if the onset of various phases of recovery in anastasis (e.g. cell proliferation) in PRs is later than in cancer cells. Nonetheless, our results do confirm that anastasis likely occurs in photoceptor cells and signs of healthy cell function appear after 48 hours of recovery, evidenced by an increase in cell proliferation.

PARP-1 and cleaved-PARP-1 protein expressions are indicative of healthy versus stressed cells. Our western blot analysis confirmed that apoptosis-induced cells have significantly greater levels of both PARP and cleaved-PARP protein compared to untreated, healthy cells. Cells allowed to recover in fresh media for 48 hours, on the other hand, showed a significant decrease in PARP and cleaved-PARP expression compared to apoptotic cells but *no* significant difference compared to untreated cells. These results expound that when allowed to recover, cells actively alter protein expression to shift to survival mechanisms. Interestingly, as mentioned previously, whilst healthy cells have normal levels PARP-1 to detect and repair DNA damage, cells with significant DNA damage have significantly elevated PARP-1 levels (Chaitanya et al., 2010). Increased activation of PARP-1 is linked to cell death and overexpression of PARP family proteins, such as tankyrase-2, causes cell toxicity (Wang et al., 2003; Kaminker et al., 2001). Overexpression of PARP is a sign of apoptosis, especially with evidence implicating apoptosis-inducing factor (AIF) as one of the downstream signaling elements in PARP-1 dependent apoptosis (Yu et al., 2002; Hong, 2024). Thus, our results indicate that control cells exhibited the expected baseline expression of PARP-1 required for

normal DNA repair. On the other hand, apoptotic (treatment-only) cells displayed significantly increased PARP-1 levels. Following recovery, PARP-1 expression in cells significantly decreased and protein levels were found to be no significantly different than those of healthy cells These findings suggest that anastasis proceeded in photoreceptor cells and that following recovery, cells were able to regain normal PARP-1 regulation.

The presence of cleaved-PARP-1 is another strong predictor and distinguisher between healthy and apoptotic cells. Evidently, a myriad of previous studies associated caspase-3 facilitated cleavage of PARP-1 with various neurodegenerative and neurological diseases (Chaitanya et al., 2010). Caspase-mediated apoptosis is characterized by the cleavage of key function and survival proteins, such as PARP-1, by caspases (Fischer et al., 2003; Kaufmann et al., 1993; Tewari et al., 1995). Consequently, increased levels of cleaved-PARP indicate greater activation of the apoptosis pathways. Our results found that healthy photoreceptors expressed the expected low baseline levels of cleaved-PARP protein, whereas apoptotic cells had significantly greater expression. After 48 hours of recovery, photoreceptors displayed significantly decreased cleaved-PARP-1 expression than during apoptosis, suggesting that the apoptotic pathway was less activated in cells undergoing anastasis. Furthermore, recovery cells and control cells were found to have no significant difference in cleaved-PARP-1 protein levels. These findings suggest that after a recovery period, photoreceptor cells were able to reverse apoptosis induction by no longer upregulating PARP-1 and cleaved-PARP-1 expression and revert their protein levels back to expected levels of healthy cells.

IER5, EGR1, and FOS were genes tested based on a paper by Sun et al., suggesting that they are part of an “anastasis profile” of gene expression changes which could serve as markers for anastasis. The exact functions and mechanisms of these genes in anastatic cells remain to be elucidated. With that being said, we found that IER5 mRNA expression was significantly greater in cells undergoing anastasis compared to both apoptotic and control cells. Another study also found hyperexpression of IER5 in anastatic cells compared to control cells (Sun et al., 2017). In regards to EGR1, it has been shown to be an anastasis marker (Sun et al., 2017), but there are contradictory reports if its expression induces apoptosis or if it is protective (Dong et al., 2022; Yi et al., 2018; Sun et al., 2017; Tang et al., 2017; Huang et al., 1998). Our results found that apoptosis-induced cells exhibited significantly less mRNA expression of EGR1 compared to control cells. However, after the stressor was removed and cells were allowed to recover for 48

hours, anastatic cells showed the same EGR1 expression as controls, suggesting that in this case EGR1 may have protective effects. Our findings differ from other studies which found that EGR1 gene expression was upregulated (Fold change > 1) compared to untreated, control cells (Tang et al., 2017; Sun et al., 2017). We also observed that FOS expression was significantly greater in recovery cells in comparison to both control and apoptotic cells. These results are similar to previous findings where some studies also reported detecting significant upregulation of FOS gene expression in anastatic cells compared to untreated, control cells (Tang et al., 2017; Sun et al., 2017).

Whilst this study does introduce a promising, novel concept to photoreceptor cells, there are still some major limitations. Primarily, anastasis has mostly been studied either in cancer cells or *in vitro*. This study, too, employs a cell culture model to evaluate and examine the mechanism. Anastasis has yet to be demonstrated in human retinal tissue, but in order to even consider therapeutic uses for anastasis, human relevance will have to be tested.

Additionally, recent studies have revealed that non-apoptotic death mechanisms — autophagy and necroptosis — are also greatly active processes involved in cell death (Murakami et al., 2013). A study by Murakami et al. observed both apoptotic and non-apoptotic pathways to have direct implications in photoreceptor cell death in retinal detachment (RD) (Murakami et al., 2013), and one by Mitter et al. indicates deficiencies in autophagy may play a role in age-related macular degeneration (AMD) (Mitter et al., 2012). Consequently, the possibility likely exists that additional death processes, on top of apoptosis, will also require regulation to achieve full neuroprotection. With that said, it seems mechanisms by which cells can reserve and survive necroptosis, which is caspase-independent, may exist (Mohammed et al., 2022; Grootjans et al., 2017). Nevertheless, because apoptotic, autophagic, and necrotic pathways are all involved in photoreceptor cell death, targeting all three mechanisms in combination is likely the most effective and promising neuroprotective strategy against retinal neurodegeneration.

Accordingly, for the overarching goal regarding treatments for substantial PR loss and resulting neurodegeneration, mechanisms protecting against all three death pathways should be examined. Even within apoptosis itself, this study only investigated the intrinsic pathway — likewise, anastasis in the extrinsic pathway remains to be elucidated. Previous studies have indicated that during apoptosis cells upregulate certain genes in preparation for anastasis, but if stress continues these mRNAs are degraded and apoptosis continues (Sun et al., 2017).

Additionally, studies propose the degree of nuclear fragmentation appears to be a potential indicator of the irreversible point of apoptosis (Tang et al., 2009). Ergo, next steps also include testing more time points along the apoptotic pathway and death cascade to determine the latest point the stressor can be removed for anastasis to still occur. Moreover, when STS was the apoptosis inducer used, Sun et al. observed the presence of 44 early-response genes in anastasis, as well as a subset even in apoptosis (Sun et al., 2017). Likewise, further studies could examine the expression of more of such markers in photoreceptor cells to gain better understanding of the mechanisms of anastasis. Potential markers of interest could include proangiogenic factors such as TGFβ, Snail1, and PGF, as they have been predicted to enrich anastasis by stimulating nutrient supply, blood vessel growth, and degradation of cellular waste — all which may be vital in recovering photoreceptors (Sun et al., 2017; Tang et al., 2018).

Limitations notwithstanding, this study also has its strengths. We demonstrated that anastasis occurs in retinal photoreceptor cells, which — when allowed to recover — regain normal morphology and cell functions.

References

Acuner Ozbabacan SE, Keskin O, Nussinov R, Gursoy A (2012) Enriching the human apoptosis pathway by predicting the structures of protein-protein complexes. J Struct Biol 179:338-346.

Alberts B, Johnson A, Lewis J, Raff M, Roberts K, Walter P (2002) Molecular Biology of the Cell, 4th edition. New York: Garland Science.

Arandjelovic S, Ravichandran KS (2015) Phagocytosis of apoptotic cells in homeostasis. Nat Immunol 16:907-917.

Barkana Y, Belkin M (2004) Neuroprotection in ophthalmology: a review. Brain Res Bull 62:447-453.

Barquilla A, Pasquale EB (2015) Eph receptors and ephrins: therapeutic opportunities. Annu Rev Pharmacol Toxicol 55:465-487.

Beere HM, Wolf BB, Cain K, Mosser DD, Mahboubi A, Kuwana T, Tailor P, Morimoto RI, Cohen GM, Green DR (2000) Heat-shock protein 70 inhibits apoptosis by preventing recruitment of procaspase-9 to the Apaf-1 apoptosome. Nat Cell Biol 2:469-475.

Branzei D, Foiani M (2008) Regulation of DNA repair throughout the cell cycle. Nat Rev Mol Cell Biol 9:297-308.

Chaitanya GV, Steven AJ, Babu PP (2010) PARP-1 cleavage fragments: signatures of cell-death proteases in neurodegeneration. Cell Commun Signal 8:31.

Chinskey ND, Besirli CG, Zacks DN (2014) Retinal cell death and current strategies in retinal neuroprotection. Curr Opin Ophthalmol 25:228-233.

Chipuk JE, Bouchier-Hayes L, Green DR (2006) Mitochondrial outer membrane permeabilization during apoptosis: the innocent bystander scenario. Cell Death Differ 13:1396-1402.

Colell A, Ricci JE, Tait S, Milasta S, Maurer U, Bouchier-Hayes L, Fitzgerald P, Guio-Carrion A, Waterhouse NJ, Li CW, Mari B, Barbry P, Newmeyer DD, Beere HM, Green DR (2007) GAPDH and autophagy preserve survival after apoptotic cytochrome c release in the absence of caspase activation. Cell 129:983-997.

Coleman ML, Sahai EA, Yeo M, Bosch M, Dewar A, Olson MF (2001) Membrane blebbing during apoptosis results from caspase-mediated activation of ROCK I. Nat Cell Biol 3:339-345.

Cooper GM (2000) The Cell: A Molecular Approach 2nd edition. National Center for Biotechnology InformationÕs Bookshelf.

Dean M, Fojo T, Bates S (2005) Tumour stem cells and drug resistance. Nat Rev Cancer 5:275-284.

Ding WX, Yin XM (2012) Mitophagy: mechanisms, pathophysiological roles, and analysis. Biol Chem 393:547-564.

Ding Y, Chen X, Liu C, Ge W, Wang Q, Hao X, Wang M, Chen Y, Zhang Q (2021) Identification of a small molecule as inducer of ferroptosis and apoptosis through ubiquitination of GPX4 in triple negative breast cancer cells. J Hematol Oncol 14:19.

Dong Y, Xu W, Li Y, Wei C, Hu Y, Hu Z, Paquet-Durand F, Jiao K (2022) Inhibition of the MAPK/c-Jun-EGR1 Pathway Decreases Photoreceptor Cell Death in the rd1 Mouse Model for Inherited Retinal Degeneration. Int J Mol Sci 23:14600.

Elliott MR, Ravichandran KS (2016) The Dynamics of Apoptotic Cell Clearance. Dev Cell 38:147-160.

Elmore S (2007) Apoptosis: a review of programmed cell death. Toxicol Pathol 35:495-516.

Enari M, Sakahira H, Yokoyama H, Okawa K, Iwamatsu A, Nagata S (1998) A caspase-activated DNase that degrades DNA during apoptosis, and its inhibitor ICAD. Nature 391:43-50.

Eskandari E, Eaves CJ (2022) Paradoxical roles of caspase-3 in regulating cell survival, proliferation, and tumorigenesis. J Cell Biol 221:e202201159.

Fabre M, Mateo L, Lamaa D, Baillif S, Pagès G, Demange L, Ronco C, Benhida R (2022) Recent Advances in Age-Related Macular Degeneration Therapies. Molecules 27:5089.

Feoktistova M, Geserick P, Leverkus M (2016) Crystal Violet Assay for Determining Viability of Cultured Cells. Cold Spring Harb Protoc 2016:pdb.prot087379.

Fischer U, Jänicke RU, Schulze-Osthoff K (2003) Many cuts to ruin: a comprehensive update of caspase substrates. Cell Death Differ 10:76-100.

Françon A, Torriglia A (2023) Cell death mechanisms in retinal phototoxicity. Journal of Photochemistry and Photobiology 15:100185.

Franza BR, Rauscher FJ, Josephs SF, Curran T (1988) The Fos complex and Fos-related antigens recognize sequence elements that contain AP-1 binding sites. Science 239:1150-1153.

Frenzel A, Grespi F, Chmelewskij W, Villunger A (2009) Bcl2 family proteins in carcinogenesis and the treatment of cancer. Apoptosis 14:584-596.

Gama V, Swahari V, Schafer J, Kole AJ, Evans A, Huang Y, Cliffe A, Golitz B, Sciaky N, Pei XH, Xiong Y, Deshmukh M (2014) The E3 ligase PARC mediates the degradation of cytosolic cytochrome c to promote survival in neurons and cancer cells. Sci Signal 7:ra67.

Geisler S, Holmström KM, Skujat D, Fiesel FC, Rothfuss OC, Kahle PJ, Springer W (2010) PINK1/Parkin-mediated mitophagy is dependent on VDAC1 and p62/SQSTM1. Nat Cell Biol 12:119-131.

Goldstein JC, Waterhouse NJ, Juin P, Evan GI, Green DR (2000) The coordinate release of cytochrome c during apoptosis is rapid, complete and kinetically invariant. Nat Cell Biol 2:156-162.

Gozzelino R, Jeney V, Soares MP (2010) Mechanisms of cell protection by heme oxygenase-1. Annu Rev Pharmacol Toxicol 50:323-354.

Green D, Kroemer G (1998) The central executioners of apoptosis: caspases or mitochondria. Trends Cell Biol 8:267-271.

Green DR (2005) Apoptotic pathways: ten minutes to dead. Cell 121:671-674.

Green DR, Kroemer G (2004) The pathophysiology of mitochondrial cell death. Science 305:626-629.

Green DR, Llambi F (2015) Cell Death Signaling. Cold Spring Harb Perspect Biol 7:a006080.

Grootjans S, Vanden Berghe T, Vandenabeele P (2017) Initiation and execution mechanisms of necroptosis: an overview. Cell Death Differ 24:1184-1195.

Gu L, Zhu N, Zhang H, Durden DL, Feng Y, Zhou M (2009) Regulation of XIAP translation and induction by MDM2 following irradiation. Cancer Cell 15:363-375.

Guo L, Li SY, Ji FY, Zhao YF, Zhong Y, Lv XJ, Wu XL, Qian GS (2014) Role of Angptl4 in vascular permeability and inflammation. Inflamm Res 63:13-22.

Gurbuxani S, Schmitt E, Cande C, Parcellier A, Hammann A, Daugas E, Kouranti I, Spahr C, Pance A, Kroemer G, Garrido C (2003) Heat shock protein 70 binding inhibits the nuclear import of apoptosis-inducing factor. Oncogene 22:6669-6678.

Harvey JW (2012) Evaluation of Leukocytic Disorders. Veterinary Hematology:122–176.

Helming L, Winter J, Gordon S (2009) The scavenger receptor CD36 plays a role in cytokine-induced macrophage fusion. J Cell Sci 122:453-459.

Holland AJ, Cleveland DW (2012) Chromoanagenesis and cancer: mechanisms and consequences of localized, complex chromosomal rearrangements. Nat Med 18:1630-1638.

Hong S, Dawson T, Dawson V (2024) PARP and the Release of Apoptosis-Inducing Factor from Mitochondria. Available at: https://www.ncbi.nlm.nih.gov/books/NBK6179/ [Accessed April 2, 2024].

Huang RP, Fan Y, deBelle I, Ni Z, Matheny W, Adamson ED (1998) Egr-1 inhibits apoptosis during the UV response: correlation of cell survival with Egr-1 phosphorylation. Cell Death Differ 5:96-106.

Ichim G, Lopez J, Ahmed SU, Muthalagu N, Giampazolias E, Delgado ME, Haller M, Riley JS, Mason SM, Athineos D, Parsons MJ, van de Kooij B, Bouchier-Hayes L, Chalmers AJ, Rooswinkel RW, Oberst A, Blyth K, Rehm M, Murphy DJ, Tait SWG (2015) Limited mitochondrial permeabilization causes DNA damage and genomic instability in the absence of cell death. Mol Cell 57:860-872.

Joza N, Susin SA, Daugas E, Stanford WL, Cho SK, Li CY, Sasaki T, Elia AJ, Cheng HY, Ravagnan L, Ferri KF, Zamzami N, Wakeham A, Hakem R, Yoshida H, Kong YY, Mak TW, Zúñiga-Pflücker JC, Kroemer G, Penninger JM (2001) Essential role of the mitochondrial apoptosis-inducing factor in programmed cell death. Nature 410:549-554.

Kalinowska M, Garncarz W, Pietrowska M, Garrard WT, Widlak P (2005) Regulation of the human apoptotic DNase/RNase endonuclease G: involvement of Hsp70 and ATP. Apoptosis 10:821-830.

Kaminker PG, Kim SH, Taylor RD, Zebarjadian Y, Funk WD, Morin GB, Yaswen P, Campisi J (2001) TANK2, a new TRF1-associated poly(ADP-ribose) polymerase, causes rapid induction of cell death upon overexpression. J Biol Chem 276:35891-35899.

Kanoh M, Takemura G, Misao J, Hayakawa Y, Aoyama T, Nishigaki K, Noda T, Fujiwara T, Fukuda K, Minatoguchi S, Fujiwara H (1999) Significance of myocytes with positive DNA in situ nick end-labeling (TUNEL) in hearts with dilated cardiomyopathy: not apoptosis but DNA repair. Circulation 99:2757-2764.

Karamitopoulou E, Cioccari L, Jakob S, Vallan C, Schaffner T, Zimmermann A, Brunner T (2007) Active caspase 3 and DNA fragmentation as markers for apoptotic cell death in primary and metastatic liver tumours. Pathology 39:558-564.

Kaufmann SH, Desnoyers S, Ottaviano Y, Davidson NE, Poirier GG (1993) Specific proteolytic cleavage of poly(ADP-ribose) polymerase: an early marker of chemotherapy-induced apoptosis. Cancer Res 53:3976-3985.

Ketelut-Carneiro N, Fitzgerald KA (2022) Apoptosis, Pyroptosis, and Necroptosis-Oh My! The Many Ways a Cell Can Die. J Mol Biol 434:167378.

Khalili AA, Ahmad MR (2015) A Review of Cell Adhesion Studies for Biomedical and Biological Applications. Int J Mol Sci 16:18149-18184.

Kim JH, Jeong IY, Lim Y, Lee YH, Shin SY (2011) Estrogen receptor beta stimulates Egr-1 transcription via MEK1/Erk/Elk-1 cascade in C6 glioma cells. BMB Rep 44:452-457.

Larsen BD, Sørensen CS (2017) The caspase-activated DNase: apoptosis and beyond. FEBS J 284:1160-1170.

Letai AG (2008) Diagnosing and exploiting cancer's addiction to blocks in apoptosis. Nat Rev Cancer 8:121-132.

Li LY, Luo X, Wang X (2001) Endonuclease G is an apoptotic DNase when released from mitochondria. Nature 412:95-99.

Liton PB, Boesze-Battaglia K, Boulton ME, Boya P, Ferguson TA, Ganley IG, Kauppinnen A, Laurie GW, Mizushima N, Morishita H, Russo R, Sadda J, Shyam R, Sinha D, Thompson DA, Zacks DN (2023) AUTOPHAGY IN THE EYE: FROM PHYSIOLOGY TO PATHOPHYSOLOGY. Autophagy Rep 2:2178996.

Los M, Mozoluk M, Ferrari D, Stepczynska A, Stroh C, Renz A, Herceg Z, Wang ZQ, Schulze-Osthoff K (2002) Activation and caspase-mediated inhibition of PARP: a molecular switch between fibroblast necrosis and apoptosis in death receptor signaling. Mol Biol Cell 13:978-988.

Malsy M, Bitzinger D, Graf B, Bundscherer A (2019) Staurosporine induces apoptosis in pancreatic carcinoma cells PaTu 8988t and Panc-1 via the intrinsic signaling pathway. Eur J Med Res 24:5.

Marchesi N, Fahmideh F, Boschi F, Pascale A, Barbieri A (2021) Ocular Neurodegenerative Diseases: Interconnection between Retina and Cortical Areas. Cells 10:2394.

Mashimo M, Onishi M, Uno A, Tanimichi A, Nobeyama A, Mori M, Yamada S, Negi S, Bu X, Kato J, Moss J, Sanada N, Kizu R, Fujii T (2021) The 89-kDa PARP1 cleavage fragment serves as a cytoplasmic PAR carrier to induce AIF-mediated apoptosis. J Biol Chem 296:100046.

Minchinton AI, Tannock IF (2006) Drug penetration in solid tumours. Nat Rev Cancer 6:583-592.

Mitter SK, Rao HV, Qi X, Cai J, Sugrue A, Dunn WA, Grant MB, Boulton ME (2012) Autophagy in the Retina: A Potential Role in Age-related Macular Degeneration. Adv Exp Med Biol 723:83-90.

Mohammed RN, Khosravi M, Rahman HS, Adili A, Kamali N, Soloshenkov PP, Thangavelu L, Saeedi H, Shomali N, Tamjidifar R, Isazadeh A, Aslaminabad R, Akbari M (2022) Anastasis: cell recovery mechanisms and potential role in cancer. Cell Commun Signal 20:81.

Momand J, Zambetti GP, Olson DC, George D, Levine AJ (1992) The mdm-2 oncogene product forms a complex with the p53 protein and inhibits p53-mediated transactivation. Cell 69:1237-1245.

Mosser DD, Caron AW, Bourget L, Meriin AB, Sherman MY, Morimoto RI, Massie B (2000) The chaperone function of hsp70 is required for protection against stress-induced apoptosis. Mol Cell Biol 20:7146-7159.

Murakami Y, Notomi S, Hisatomi T, Nakazawa T, Ishibashi T, Miller JW, Vavvas DG (2013) Photoreceptor cell death and rescue in retinal detachment and degenerations. Prog Retin Eye Res 37:114-140.

Narula J, Pandey P, Arbustini E, Haider N, Narula N, Kolodgie FD, Dal Bello B, Semigran MJ, Bielsa-Masdeu A, Dec GW, Israels S, Ballester M, Virmani R, Saxena S, Kharbanda S (1999) Apoptosis in heart failure: release of cytochrome c from mitochondria and activation of caspase-3 in human cardiomyopathy. Proc Natl Acad Sci U S A 96:8144-8149.

National Center for Biotechnology Information (2024) PubChem Compound Summary for CID 44259, Staurosporine. Available at: https://pubchem.ncbi.nlm.nih.gov/compound/44259 [Accessed April 2, 2024].

Okatsu K, Saisho K, Shimanuki M, Nakada K, Shitara H, Sou YS, Kimura M, Sato S, Hattori N, Komatsu M, Tanaka K, Matsuda N (2010) p62/SQSTM1 cooperates with Parkin for perinuclear clustering of depolarized mitochondria. Genes Cells 15:887-900.

Olivares-González L, Velasco S, Campillo I, Rodrigo R (2021) Retinal Inflammation, Cell Death and Inherited Retinal Dystrophies. Int J Mol Sci 22:2096.

Pandey P, Farber R, Nakazawa A, Kumar S, Bharti A, Nalin C, Weichselbaum R, Kufe D, Kharbanda S (2000) Hsp27 functions as a negative regulator of cytochrome c-dependent activation of procaspase-3. Oncogene 19:1975-1981.

Pardue MT, Allen RS (2018) Neuroprotective strategies for retinal disease. Prog Retin Eye Res 65:50-76.

Patel C, Pande S, Sagathia V, Ranch K, Beladiya J, Boddu SHS, Jacob S, Al-Tabakha MM, Hassan N, Shahwan M (2023) Nanocarriers for the Delivery of Neuroprotective Agents in the Treatment of Ocular Neurodegenerative Diseases. Pharmaceutics 15:837.

Paul C, Manero F, Gonin S, Kretz-Remy C, Virot S, Arrigo AP (2002) Hsp27 as a negative regulator of cytochrome C release. Mol Cell Biol 22:816-834.

Poon HK, Tso MO, Lam TT (2000) c-Fos protein in photoreceptor cell death after photic injury in rats. Invest Ophthalmol Vis Sci 41:2755-2758.

Radoshevich L, Murrow L, Chen N, Fernandez E, Roy S, Fung C, Debnath J (2010) ATG12 conjugation to ATG3 regulates mitochondrial homeostasis and cell death. Cell 142:590-600.

Ravagnan L, Gurbuxani S, Susin SA, Maisse C, Daugas E, Zamzami N, Mak T, Jäättelä M, Penninger JM, Garrido C, Kroemer G (2001) Heat-shock protein 70 antagonizes apoptosis-inducing factor. Nat Cell Biol 3:839-843.

Riedl SJ, Shi Y (2004) Molecular mechanisms of caspase regulation during apoptosis. Nat Rev Mol Cell Biol 5:897-907.

Salvucci O, Tosato G (2012) Essential roles of EphB receptors and EphrinB ligands in endothelial cell function and angiogenesis. Adv Cancer Res 114:21-57.

Sayyad Z, Sirohi K, Radha V, Swarup G (2017) 661W is a retinal ganglion precursor-like cell line in which glaucoma-associated optineurin mutants induce cell death selectively. Sci Rep 7:16855.

Schmidt KG, Bergert H, Funk RH (2008) Neurodegenerative diseases of the retina and potential for protection and recovery. Curr Neuropharmacol 6:164-178.

Sheng M, Greenberg ME (1990) The regulation and function of c-fos and other immediate early genes in the nervous system. Neuron 4:477-485.

Simons M, Gordon E, Claesson-Welsh L (2016) Mechanisms and regulation of endothelial VEGF receptor signalling. Nat Rev Mol Cell Biol 17:611-625.

Slee EA, Adrain C, Martin SJ (2001) Executioner caspase-3, -6, and -7 perform distinct, non-redundant roles during the demolition phase of apoptosis. J Biol Chem 276:7320-7326.

Stillwell W (2016) Chapter 19 – Membrane Transport. In: An Introduction to Biological Membranes, pp423-251. Elsevier Science.

Sun G, Guzman E, Balasanyan V, Conner CM, Wong K, Zhou HR, Kosik KS, Montell DJ (2017) A molecular signature for anastasis, recovery from the brink of apoptotic cell death. J Cell Biol 216:3355-3368.

Sun G, Montell DJ (2017) Q&A: Cellular near death experiences-what is anastasis. BMC Biol 15:92.

Tang HM, Talbot CC, Fung MC, Tang HL (2017) Molecular signature of anastasis for reversal of apoptosis. F1000Res 6:43.

Tang HM, Tang HL (2018) Anastasis: recovery from the brink of cell death. R Soc Open Sci 5:180442.

Tang HL, Tang HM, Hardwick JM, Fung MC (2015) Strategies for tracking anastasis, a cell survival phenomenon that reverses apoptosis. J Vis Exp 96:51964.

Tang HL, Tang HM, Mak KH, Hu S, Wang SS, Wong KM, Wong CS, Wu HY, Law HT, Liu K, Talbot CC, Lau WK, Montell DJ, Fung MC (2012) Cell survival, DNA damage, and oncogenic transformation after a transient and reversible apoptotic response. Mol Biol Cell 23:2240-2252.

Tang HL, Yuen KL, Tang HM, Fung MC (2009) Reversibility of apoptosis in cancer cells. Br J Cancer 100:118-122.

Taylor RC, Cullen SP, Martin SJ (2008) Apoptosis: controlled demolition at the cellular level. Nat Rev Mol Cell Biol 9:231-241.

Tewari M, Quan LT, O'Rourke K, Desnoyers S, Zeng Z, Beidler DR, Poirier GG, Salvesen GS, Dixit VM (1995) Yama/CPP32 beta, a mammalian homolog of CED-3, is a CrmA-inhibitable protease that cleaves the death substrate poly(ADP-ribose) polymerase. Cell 81:801-809.

Usategui-Martin R, Fernandez-Bueno I (2021) Neuroprotective therapy for retinal neurodegenerative diseases by stem cell secretome. Neural Regen Res 16:117-118.

van den Eijnde SM, van den Hoff MJ, Reutelingsperger CP, van Heerde WL, Henfling ME, Vermeij-Keers C, Schutte B, Borgers M, Ramaekers FC (2001) Transient expression of phosphatidylserine at cell-cell contact areas is required for myotube formation. J Cell Sci 114:3631-3642.

Villa E, Proïcs E, Rubio-Patiño C, Obba S, Zunino B, Bossowski JP, Rozier RM, Chiche J, Mondragón L, Riley JS, Marchetti S, Verhoeyen E, Tait SWG, Ricci JE (2017) Parkin-Independent Mitophagy Controls Chemotherapeutic Response in Cancer Cells. Cell Rep 20:2846-2859.

Wang B, Guo H, Yu H, Chen Y, Xu H, Zhao G (2021) The Role of the Transcription Factor EGR1 in Cancer. Front Oncol 11:642547.

Wang H, Shimoji M, Yu SW, Dawson TM, Dawson VL (2003) Apoptosis inducing factor and PARP-mediated injury in the MPTP mouse model of Parkinson's disease. Ann N Y Acad Sci 991:132-139.

Ward TH, Cummings J, Dean E, Greystoke A, Hou JM, Backen A, Ranson M, Dive C (2008) Biomarkers of apoptosis. Br J Cancer 99:841-846.

Wheway G, Nazlamova L, Turner D, Cross S (2019) 661W Photoreceptor Cell Line as a Cell Model for Studying Retinal Ciliopathies. Front Genet 10:308.

Williams M, Lyu MS, Yang YL, Lin EP, Dunbrack R, Birren B, Cunningham J, Hunter K (1999) Ier5, a novel member of the slow-kinetics immediate-early genes. Genomics 55:327-334.

Yang C, Wang Y, Hao C, Yuan Z, Liu X, Yang F, Jiang H, Jiang X, Zhou P, Ding K (2016) IER5 promotes irradiation- and cisplatin-induced apoptosis in human hepatocellular carcinoma cells. Am J Transl Res 8:1789-1798.

Yi EH, Xu F, Li P (2018) (3R)-5,6,7-trihydroxy-3-isopropyl-3-methylisochroman-1-one alleviates lipoteichoic acid-induced photoreceptor cell damage. Cutan Ocul Toxicol 37:367-373.

Yu SW, Wang H, Poitras MF, Coombs C, Bowers WJ, Federoff HJ, Poirier GG, Dawson TM, Dawson VL (2002) Mediation of poly(ADP-ribose) polymerase-1-dependent cell death by apoptosis-inducing factor. Science 297:259-263.

Yu Z, Correa VSMC, Efstathiou NE, Albertos-Arranz H, Chen X, Ishihara K, Iesato Y, Narimatsu T, Ntentakis D, Vavvas DG (2022) UVA induces retinal photoreceptor cell death via receptor interacting protein 3 kinase mediated necroptosis. Cell Death Discov 8:489.

Zhang R, Yang D, Zhou C, Cheng K, Liu Z, Chen L, Fang L, Xie P (2012) β-actin as a loading control for plasma-based Western blot analysis of major depressive disorder patients. Anal Biochem 427:116-120.

Appendix

Raw Data from MTT Assay at Varying Drug Concentrations

Control	0.05µM	0.1µM	0.2µM	0.3µM	0.4µM	0.5µM
100	70.35519	59.28962	63.25137	57.24044	37.43169	19.2623
100	69.95769	62.76446	63.04654	60.6488	43.15938	22.28491
100	74.44279	65.82467	69.39079	65.3789	45.46805	31.20357
100	79.23323	69.32907	75.07987	68.37061	31.62939	33.86581
100	68.07947	52.98013	52.31788	53.24503	23.17881	24.37086
100	72.94618	56.37394	57.64873	56.79887	24.36261	25.92068

Raw Data from Crystal Violet Assay at Varying Drug Concentrations

Control	0.05µM	0.1µM	0.2µM	0.3µM	0.4µM
100	60.17029328	58.75118259	54.99842321	50.61494797	45.53768527
100	60.44025157	59.62264151	57.57861635	48.71069182	42.29559748
100	87.50584932	89.98596163	97.09873655	70.4258306	81.60973327
100	76.52851867	80.05744768	79.68814116	66.43414034	59.25318014
100	75.50857599	84.52333466	64.02074192	64.81850818	53.64978061
100	76.27603103	72.31523071	63.25030625	67.33360555	70.11024908

Raw Data from Crystal Violet Assay after 24hrs Recovery

Treatment group.

Control	100	100	100	100	100	100
0.02µM	84.42467	84.1068	90.08264	71.64654	80.29243	79.78385
0.03µM	60.45772	62.74634	67.57788	64.78067	66.815	64.78067
0.04µM	53.21043	58.10553	62.11062	61.34774	65.60712	64.58996
0.05µM	46.85315	45.39097	43.03878	42.27591	52.89256	51.8754

Anastasis - Recovery (24hrs) group.

Control	100	100	100	100	100	100
0.02µM	80.06206	80.52754	85.49263	85.02715	80.44996	81.22576
0.03µM	73.50659	72.96354	68.96819	68.03724	59.8526	59.34833
0.04µM	70.28704	69.16214	66.09775	69.00698	58.99922	60.35687
0.05µM	45.49263	35.61404	29.0384	39.90344	39.41198	38.76259

End Point group.

Control	100	100	100	100	100	100
0.02µM	56.0419	86.32789	75.33265	74.45514	79.70348	51.82882
0.03µM	50.16835	69.87296	72.72262	72.57983	70.80777	51.2436
0.04µM	43.02282	69.14701	55.88536	58.74303	62.93456	43.48939
0.05µM	30.49009	33.1337	29.02866	27.83376	21.86094	39.48061

Raw Data from Crystal Violet Assay after 48hrs Recovery

Treatment group.

Control	100	100	100	100	100	*100**
0.02µM	56.53595	78.66498	81.37441	77.5463	82.51366	*79.78385**
0.03µM	65.45285	44.52894	62.36967	42.96296	73.72081	*64.78067**
0.04µM	35.57423	81.58006	51.37441	46.2963	53.50224	*64.58996**
0.05µM	30.39216	31.09421	34.02844	37.68519	42.57327	*51.8754**

Anastasis - Recovery (48hrs) group.

Control	100	100	100	100	100	*100**
0.02µM	94.96366	95.09124	94.43582	92.69395	93.71311	*81.22576**
0.03µM	79.9325	93.18941	93.27122	93.09566	87.40056	*59.34833**
0.04µM	89.09657	88.17785	93.71118	86.06578	85.91224	*60.35687**
0.05µM	78.71236	74.14546	82.50518	80.1406	68.89915	*38.76259**

End Point group.

Control	100	100	100	100	100	*100**
0.02µM	76.40187	68.15729	56.4441	57.77052	62.86887	*51.82882**
0.03µM	72.19626	63.96813	78.67495	43.4346	66.41006	*51.2436**
0.04µM	60.64382	70.34181	58.20393	52.7994	58.71183	*43.48939**
0.05µM	43.71755	52.17168	56.90994	55.36028	50.39774	*39.48061**

Raw Data from Western Blot of PARP after 48hrs Recovery

PARP

Control	**Treatment**	**Treatment + Recovery**
1	2.541243	1.11811
1	1.544441	0.895587
1	1.812122	0.890831

Cleaved-PARP

Control	**Treatment**	**Treatment + Recovery**
1	1.978329	0.236763
1	2.585321	0.803743
1	1.487752	1.013938

Raw Data from RT-PCR after 48hrs Recovery

IER5

Control	Treatment	Treatment + Recovery	End Point
1	3.93953475759807	6.37463898484774	1.63879184501778
1	4.0675966417752	5.34461047299617	1.54514557909436

EGR1

Control	Treatment	Treatment + Recovery	End Point
1	0.633384444403067	0.947724351149127	0.73347184870588
1	0.554721711095046	0.849837464982425	0.80718966809818

FOS

Control	Treatment	Treatment + Recovery	End Point
1	1.56969400675752	2.77133653919264	1.20194760802633
1	1.74432364532369	3.2288375094763	1.92568357129139